Ice accretion on cylinders and wires / Givrage des cylindres et des câbles

Makkonen, L. J.; Stallabrass, J. R.

Technical Report (National Research Council of Canada. Division of Mechanical Engineering. Low Temperature Laboratory); no. TR-LT-005, 1984-07

Technical Report

Rapport technique

1984/07

TR-LT-005
NRC NO. 23649

ICE ACCRETION ON CYLINDERS AND WIRES

L.J. Makkonen, J.R. Stallabrass

Division of
Mechanical Engineering

Division de
génie mécanique

National Research Council Canada
Conseil national de recherches Canada

Canada

UNLIMITED
UNCLASSIFIED

ILLIMITÉ
NON CLASSIFIÉ

ICE ACCRETION ON CYLINDERS AND WIRES

GIVRAGE DES CYLINDRES ET DES CÂBLES

L.J. Makkonen
J.R. Stallabrass

Technical Report

1984/07

Rapport technique

TR-LT-005
NRC NO. 23649

T. R. Ringer, Head/Chef
Low Temperature Laboratory/
Laboratoire des basses températures

E. H. Dudgeon
Director/
Directeur

ACKNOWLEDGEMENT

The authors would like to thank Dr. G. Isaac of the Atmospheric Environment Service of Canada for the loan of the FSSP, and J.W. Strapp for his help, particularly in processing the FSSP data. They also wish to thank Dr. S.F. Ackley and Mr. J.W. Govoni of the U.S. Army Cold Regions Research and Engineering Laboratory for supplying the Mt. Washington icing data [Refs. 15 and 32]. This work was carried out while one of the authors (L. Makkonen) was working under the Government of Canada Visiting Fellowship programme instituted by the Natural Sciences and Engineering Research Council.

ABSTRACT

The theory of icing rate on cylindrical structures was verified against experimental data. The experiments were made in an icing wind tunnel using both smooth, slowly rotating cylinders and wires with a torsional stiffness corresponding to that of transmission line cables. These experiments, made in dry growth conditions (rime), showed excellent agreement with the results of a time-dependent numerical icing model. A forward scattering spectrometer probe (FSSP) was used, in addition to the oil slide method, in measuring the droplet size in the spray. A comparison between the two methods showed that the customarily used oil slide method seriously overestimates the median volume diameter d_m at large droplet sizes. The ice densities measured on the rotating cylinders were higher than those predicted by the model. This results from the fact that d_m measured with the oil slide has been used as the basis of the Macklin ice density parameter. A new equation for the density of accreted ice is proposed. Comparisons between the model results and previous icing wind tunnel tests and experimental results from the natural environment show that the theoretical model predicts well the icing rate in wet growth conditions (glaze) also.

CONTENTS

ILLUSTRATIONS

Figure

ILLUSTRATIONS (Cont'd)

CONTENTS (Cont'd)

ILLUSTRATIONS (Cont'd)

TABLES

ICE ACCRETION ON CYLINDERS AND WIRES

1.0 INTRODUCTION

Ice accretion on wires and other cylindrical structures is a serious problem in cold regions and causes huge economic losses and operational difficulties, particularly in the power industry [Ref. 1]. Therefore, considerable efforts towards better understanding of the physics of icing have been made in the hope of developing methods of estimating the rate of formation of ice loads on wires [Refs. 2, 3, 4, 5, 6, 7; and others].

There are several problems that have seriously hampered the development of the modeling of the icing process:

- The complexity of the physics of icing. The icing of an object involves several feed-back mechanisms and non-linear relationships between the icing rate and the various factors affecting it.

- The difficulties in assessing the input parameters. Modeling of icing requires such input parameters as the liquid water content and droplet size of the fog or cloud. There are considerable technical problems in measuring these quantities accurately, even under laboratory conditions. The icing rate is very sensitive to variations in the cloud physical parameters.

- The lack of experimental data. Precise quantitative verification of the theoretical models of icing has been virtually impossible, because of the above mentioned difficulties in measuring the input parameters. Moreover, these input parameters are highly interrelated in the natural environment. There are practical problems involved in measuring the icing rate, also.

Recently Makkonen [Ref. 8] presented a time-dependent numerical model of icing on wires which essentially handles the icing wire as a growing, slowly rotating circular cylinder. This idea is based on the observations that ice deposits on transmission line cables usually have nearly cylindrical shapes [Fig. 1 - reproduced with permission from Ref. 34] and on the results which indicate that the icing rate is not very sensitive to small deviatons from the cylindrical shape [Refs. 9 and 10]. The purpose of the report is to verify the theory of icing on cylindrical objects and provide additional experimental data on the characteristics of ice accretion. The theoretical model verified is that by Makkonen [Ref. 8] which is modified so that the recent development in the calculation of the heat transfer coefficient of a rough cylinder [Ref. 11] is included.

Laboratory experiments in the National Research Council's icing wind tunnel were conducted for this report using smooth, evenly rotating circular cylinders to test the validity of the basic theoretical assumptions that have been used as a basis of measuring the microphysical properties of clouds [e.g. Refs. 12, 13]. Experiments were also made using transmission line cables with realistic torsional stiffness to test the accuracy of the theory in the practical application of power line icing. Considerable attention in the experiments was paid to secure the accurate determination of the droplet size. To achieve this the forward scattering spectrometer probe (FSSP) was installed in the wind tunnel and used for droplet size calibrations.

2.0 THE MODEL

2.1 General Description

The icing intensity I is the rate of increase in the mass of ice divided by the portion of surface area of the ice deposit that faces the wind. On a circular cylinder the icing intensity is

$$I = \frac{2}{\pi} E n v w, \qquad (1)$$

where E is the collection efficiency, i.e., the ratio of the mass flow of the impinging water droplets to the mass flow that would be experienced by the surface if the droplets were not deflected in the air stream, n is the freezing fraction, i.e., the ratio of the icing intensity to the mass flow of the impinging water droplets, v is the wind speed and w is the liquid water content in the air. The quantities I, E and n in Eq. (1) are the overall values for the part of the object surface that faces the wind. In the model the ice deposit is supposed to maintain a circular form during the icing process due to rotation. The rotation is assumed slow enough so that there is no icing on the lee side of the object, even in wet growth. This is the case when considering the laboratory experiments presented in this report and when considering the icing of transmission line cables which rotate slowly due to the weight of the accreting ice [Ref. 7] resulting in fairly cylindrical ice shapes [Refs. 14 and 15].

Ice growth is considered wet when $n < 1$, which means that there is some run-off from the ice deposit as a whole. This run-off water is assumed shed into the wind at the edges of the cylinder. In dry growth $n = 1$ and there is no run-off from the deposit, although the local freezing fraction may be less than unity near the stagnation line.

During the ice accretion process on a structure the diameter of the icing object changes, and therefore E and n depend on time τ. When the atmospheric conditions are kept unchanged, it

follows from Eq. (1) that the ice load M_i per unit length of the wire at time τ_i is

$$M_i = \int_0^{\tau_i} I(\tau)\ \frac{\pi}{2}\ D(\tau)\ d\ \tau = v\ w \int_0^{\tau_i} E(\tau)\ n(\tau)\ D(\tau)\ d\ \tau \qquad (2)$$

The calculations of the model are made in a step-wise manner as shown in a schematic description of the model in Fig. 2. For each time-step i the collection efficiency E_i is calculated as explained in chapter 2.2 and the freezing fraction n_i is determined from the heat balance of the icing surface as explained in chapter 2.3. Then the icing intensity I_i is obtained from Eq. (1), and the ice load M_i, where the sub-index i refers to the time-step, is

$$M_i = M_{i-1} + I_{i-1}\ \frac{\pi}{2}\ D_{i-1}\ \Delta\tau, \qquad (3)$$

The ice deposit diameter D_i corresponding to the ice mass M_i is calculated from

$$D_i = \left(\frac{4(M_i - M_{i-1})}{\pi\ \rho_i} + D_{i-1}^{\ 2} \right)^{1/2} \qquad (4)$$

Introducing Eq. (4) means that the cross-sectional area of the ice deposit in the mean is assumed to be that of a cylindrical deposit having the same ice mass.

Eq. (4) includes the density of ice, ρ_i, accreted during the time-step i. This density is calculated in a sub-routine which is explained in chapter 2.4 The time-step $\Delta\tau$ of one minute is used in the calculations.

2.2 Collection Efficiency

First, the collection efficiency E_m based on the median volume diamter of the droplet distribution is determined. The calculation is based on the numerical solution of Langmuir and Blodgett [Ref. 16] for the dimensionless equation of motion of a droplet in an airflow.

The following fits to the numerical data of Langmuir and Blodgett are used in the model

$$E_m = 0.5\ [\log_{10}\ (8\ K_0)]^{1.6} \quad \text{for } K_0 \leqslant 0.8 \qquad (5)$$

$$E_m = K_0^{\ 1.1}\ (K_0^{\ 1.1} + 1.426)^{-1} \quad \text{for } K_0 > 0.8, \qquad (6)$$

where

$$K_0 = K \left[0.087 \, Re_d^{(0.76 \, Re_d^{-0.027})} + 1 \right]^{-1} \quad (6)$$

Here, K is the inertia parameter defined as

$$\rho_w \, v \, d^2 / 9 \mu D \quad (7)$$

and Re_d is the droplet Reynolds number based on the free stream velocity v.

$$Re_d = \frac{\rho_a d \, v}{\mu} \quad (8)$$

Here, d is the droplet diameter, D the cylinder diameter, ρ_w the water density, μ the absolute viscosity of air, and ρ_a the air density.

The calculation of E_m is made using the median volume diameter d_m of the droplets. In natural conditions, however, the icing cloud is not monodisperse, but has a certain droplet distribution. This means that the "real" collection efficiency E should be calculated separately for each size category, and the value of E is then the sum of these collection efficiencies multiplied by the fraction of the total liquid water content represented by that size. In order to take this into account the collection efficiency is corrected using an empirical equation [Ref. 8], so that

$$E = 0.69 \, E_m^{0.67} + 0.31 \, E_m^{1.67} \quad (9)$$

2.3 Freezing Fraction

The freezing fraction n is calculated from the heat balance of the icing surface, which in this case is the front half of the cylindrical ice deposit. Accordingly, the equation for the freezing fraction becomes

$$n = \frac{\pi h}{2E \, v \, w \, L_f} \left[-t_a + \frac{k L_e}{c_p p_a} (e_0 - e_a) - \frac{r v^2}{2 c_p} \right] - \frac{t_a}{L_f} \left(c_w + \frac{\pi \sigma a}{2E \, v \, w} \right) \quad (10)$$

The derivation of Eq. (10) is given in [Ref. 8].

In Eq. (10), h is the convective heat transfer coefficient, w is the liquid water content in air, L_f the latent heat of fusion at 0°C, t_a the air temperature (in °C), k = 0.62, L_e the latent heat of evaporation at 0°C, c_p the specific heat of air at constant pressure, and p_a the air pressure, e_0 and e_a are the saturation water vapour pressures over water at 0°C and at t_a respectively, r is the overall recovery factor, c_w the specific heat of water, σ the Stefan-Boltzmann constant, and $a = 8.1 \times 10^7 \, K^3$.

The overall heat transfer coefficient h in Eq. (10) is calculated using a separate numerical boundary-layer model of heat transfer from a rough cylinder. The modeling of h is explained in detail in Reference 11. This requires an estimate of the roughness element height at the ice surface, in addition to the cylinder diameter, wind speed and air temperature, as input.

2.4 Ice Density

In the time dependent modeling of icing, the growth at the object diameter needs to be related to the mass of ice using the density ρ of the accreting ice (Eq. (4)). This requires a parametrization of ρ by the input parameter of the model.

In the model Macklin's [Ref. 17] density parameter

$$R = (-v_0\, d_m/2\, t_s), \tag{11}$$

is used. Here d_m is the median volume diameter of the droplets (μm), V_0 is the impact speed of the droplets (m s^{-1}) at the stagnation region calculated according to Langmuir and Blodgett [Ref. 16] using the median volume droplet diameter d_m, and t_s is the mean surface temperature of the ice deposit (°C). The ice density ρ (g cm^{-3}) is determined from Eq. (12) which is based on Macklin's laboratory experiments and on the measurements in natural icing conditions by Bain and Gayet [Ref. 18].

$$\begin{aligned}
&\rho = 0.1 && \text{for } R \leqslant 0.9 \\
&\rho = 0.11\, R^{0.76} && \text{for } 0.9 < R \leqslant 10 \\
&\rho = R(R + 5.61)^{-1} && \text{for } 10 < R \leqslant 60 \\
&\rho = 0.92 && \text{for } R > 60
\end{aligned} \tag{12}$$

For the droplet impact speed v_0 in Eq. (11) the formulas

$$\begin{aligned}
v_0 &= v\,[-0.174 + 1.464\, K_0 - 0.816\, K_0^2] && \text{for } K_0 \leqslant 0.55 \\
v_0 &= v\,[0.561 + 0.592 \log_{10} K_0 - 0.26 (\log_{10} K_0)^2] && \text{for } K_0 > 0.55
\end{aligned} \tag{13}$$

based on the solutions of Langmuir and Blodgett [Ref. 16] are used.

The mean surface temperature t_s is solved numerically from the heat balance equation of the dry growth process [Ref. 8].

$$\frac{2}{\pi} E\, v\, w\, (L_f + c_w t_a - c_i t_s) = h\, [(t_s - t_a) + \frac{k L_s}{c_p p_a} (e_s - e_a) - \frac{r v^2}{2 c_p}] + \sigma\, a\, (t_s - t_a), \tag{14}$$

where c_i is the specific heat of ice, L_s is the latent heat of sublimation at t_s and e_s is the saturation water vapour pressure with respect to ice at the temperature t_s.

The total ice deposit density ρ_i for the time step i is finally obtained from Eq. (15)

$$\bar{\rho}_i = 4\ M_i\ (\pi\ D_i^2 - \pi\ D_0^2\ )^{-1}, \qquad (15)$$

where D_0 is the initial wire diameter.

3.0 EXPERIMENTAL PROCEDURES

3.1 Icing Wind Tunnel

The cylinder and wire icing experiments were made in the icing wind tunnel of the Low Temperature Laboratory, National Research Council of Canada [Fig. 3]. A good description of this facility is given in Reference 19. The present configuration however differs from that described in two respects.

First, because of the very low water flow rates required to generate the low liquid water contents at the low velocities of the tests, a single atomizing spray nozzle placed on the tunnel centreline was employed instead of the array of four nozzles normally used. This resulted in a rather less uniform distribution of spray concentration across the tunnel test section, with a maximum at or close to the tunnel centreline. However, all test results were based on average measurements made in the centre 10 cm of the 30.5 x 30.5 cm test section where liquid water content measurements showed that the concentration was most uniform.

Secondly, since tunnel blockage effects in some of the tests (up to 25% blockage) were expected to be present, plenum chambers with perforated walls were installed in place of the test section floor and ceiling, to give a test section porosity of 10% [Ref. 26]. Two tests with 25% blockage, without and with the porous plenum chambers, but otherwise identical conditions, showed no significant difference in the icing characteristics on a 7.61 cm diameter cylinder at 36 m/s airspeed, suggesting that blockage effects do not have a significant effect on droplet trajectories in the conditions of the tests. However, the perforated walls were used for all tests.

3.2 Measurement of Parameters

Because of the low air velocities used in these tests (between 20 and 36 m/s) the usual airspeed indicator and aneroid dial manometer used for velocity measurement were too insensitive. Accordingly, a water micro-manometer, readable to 0.025 mm H_2O, was used to measure the dynamic pressure in the tunnel test section.

At all test velocities, the turbulence intensity in the tunnel working section was 3.5 ± 0.2%.

The tunnel air total temperature was controlled and measured by the automatic temperature controller on the wind tunnel, which controlled the temperature to better than ±0.3°C of the set point. The static temperature in the test section (as listed in Tables 1 and 2) is lower than the total temperature, owing to the adiabatic expansion of the air accelerating within the contraction, the depression being about 0.2°C at 20 m/s and 0.65°C at 36 m/s.

Liquid water content was measured using the single rotating cylinder method [Ref. 20]. Tests were run at a series of spray nozzle settings of water flow rate and atomizing air pressure, estimated from prior calibrations to give liquid water contents of about 0.15 gm^{-3} and 0.3 gm^{-3} at various droplet sizes. At the chosen spray nozzle settings, confirmatory rotating cylinder measurements were made at tunnel air temperatures lower than -10°C to ensure that the Ludlam limit was not exceeded. The liquid water content values employed are the mean of several measurements (4 to 10) at each spray nozzle setting, and had a standard deviation of ± 0.02 gm^{-3}.

The conventional means of measuring the size of the spray droplets in the icing wind tunnel has been by means of the oiled slide method. This method is described in detail in Reference 21. However, in recent years, several workers [Refs. 22, 23 & 24] have criticized the method on the grounds that it overestimates the droplet size by a factor of 1.5 or more. This criticism was reinforced by the results of these tests on wires and cylinders when it was found that icing calculations using the droplet size determined by oiled slide measurements consistently overestimated the accreted ice mass.

In order to resolve this problem, comparative droplet size measurements were made in the wind tunnel with the oiled slide and with a Forward Scattering Spectrometer Probe (FSSP), manufactured by Particle Measurement Systems, Boulder, Colorado, USA, and kindly loaned by the Atmospheric Environment Service of Canada. This FSSP has undergone considerable calibrations and was one of the subject probes (serial #2) in the studies reported in Reference 25, thus engendering reasonable confidence in the accuracy of its measurements. It is accordingly assumed that the FSSP results are a measure of the true droplet size in the spray, although doubts concerning the absolute accuracy of the FSSP measurements may still be expressed.

The complete results of this comparison will be the subject of a separate report, but the significant result of relevance to this report is illustrated in Figure 4. Clearly, the criticisms levelled at the oiled slide method appear justified. The ratio between the oiled slide and the FSSP size results is not a constant, but increases from 1.0 at a median volume diameter (MVD) of

12 μm to about 2 for an FSSP MVD value of 20 μm, according to the best least squares fit to the data points:

$$d_m(\text{oil slide}) = 3.68\ d_m(\text{FSSP}) - 32.3 \qquad (16)$$

The correlation coefficient of the data set is 0.96. The inverse of equation (16), i.e.

$$d_m(\text{FSSP}) = 8.8 + 0.27\ d_m(\text{oil slide}) \qquad (17)$$

may be used to derive the equivalent FSSP droplet median volume diameter from the results of oiled slide measurements.

3.3 Rotating Cylinders

Icing tests were made on rotating cylinders of four different diameters, 1.024 cm, 3.183 cm, 4.440 cm and 7.609 cm. The speed of rotation was 2 revolutions per minute.

To facilitate measurements, particularly that of weighing a known length of the ice accretion, the cylinders were made in three parts, such that the central part, of length 10 cm, could be separated from the two outer parts [Fig. 5]. Figure 6 shows how cleanly the ice accretion on the central part separated.

The three larger cylinders were made of aluminum tubing, all having a wall thickness of 0.159 cm. The smallest cylinder, dia. 1.024 cm, was of stainless steel pipe and had a wall thickness of 0.173 cm. In all cases the surface finish was that of the "as supplied" tube or pipe, and could be considered aerodynamically smooth in the present experimental conditions.

The duration of the test runs were chosen to give a relatively small, yet measurable ice thickness. Thus, times of 30, 40 and 50 minutes were chosen for the 1.024, 3.183 and 4.440 cm diameter cylinders respectively, giving ice thicknesses of between about 1 mm and 3 mm. A 50-minute duration was chosen for the 7.609 cm diameter also, resulting in slightly smaller ice thicknesses, i.e. between about 0.6 mm and 2.5 mm.

The overall diameter of the ice deposits on the three smaller cylinders was measured with a cooled vernier caliper, while a micrometer was used for the largest cylinder. The ice mass was determined by weighing the central part of the cylinder together with its accumulated ice and subtracting the weight of the cylinder. The three smaller cylinders were measured on a precision balance accurate to 1 mg. The largest cylinder was too heavy for this balance and was weighed on a balance scaled in 1 g increments, but visually interpolated to 0.1 g. Thus, because of the lower accurcy of mass determination, and because of the smaller ice thickness, the ice density determinations on the 7.609 cm diameter cylinder are considered to be of lower precision than those for the other cylinders.

3.4 Wires

The experiments on wires were made on two simulated wire models [Fig. 7] of nominal wire diameters 1 cm and 4 cm respectively. To simulate the rotation of the wires under the influence of the ice accretion, the model wires were set in bearings in the tunnel walls and attached to a helical spring having a spring constant such that the wire model would simulate the mid-point of a representative transmission span.

The 1 cm wire was constructed by wrapping 9 strands of 0.236 cm diameter copper wire on a core consisting of a steel rod of 0.476 cm diameter, resulting in a wire of overall diameter of 0.948 cm. The model wire was assumed to represent a section of a wire having a torsional stiffness of 4.13 Nm^2/rad (10 ft^2lb/rad) and located at the centre of a 150 m span. Its torsional resistance was supplied by a spring having a spring constant of 7.6 x 10^{-3} Nm/rad.

The 4 cm wire was constructed by wrapping 27 strands of 0.405 cm diameter aluminum wire on a core of stainless steel pipe of 3.215 cm diameter, resulting in a wire of overall diameter 4.02 cm. A torsional stiffness of 413 Nm^2/rad (1000 ft^2lb/rad) and a cable span of 460 m were assumed, resulting in a required spring constant of 9.6 x 10^{-3} Nm/rad to provide a representative torsional resistance at mid-span.

With the exception of the first test on the 1 cm wire, the duration of which was 10 hours, all test runs were made for a duration of 4 hours. The rotation of the wire under the influence of gravitational and aerodynamic forces had to be assisted by some tapping of the wire end projecting through the tunnel wall, in order to overcome the friction of the bearings. The angle of rotation was periodically noted.

At the completion of each hour, the test was interrupted to measure the mean diameter of the accretion and its weight. At the completion of the test, the ice was removed from the wire by heating the wire slightly to melt the interface sufficiently to slide the ice off, and the weight of the central 10 cm was determined.

4.0 RESULTS AND DISCUSSION

4.1 The Rotating Cylinders

4.1.1 Collection efficiency

The test conditions, the results and the corresponding model simulation outputs for the rotating cylinder experiments are given in Table 1. The number of the rotating cylinder tests with separate experimental conditions is 33. For some experimental conditions two (3 cases) or three (2 cases) tests were run to check

the repeatability of the experiments. In these cases the mean values of the test results are given in Table 1 and are used in the analysis of the results. The deviation in the resulting ice amount in the tests that were repeated was within 15%. The ice density was reproducible to an accuracy better than 10%. These deviations originate from measurement errors and the fact that, although the test conditions were continuously monitored, there may have been small variations in the air and water pressures, for example.

The duration of the rotating cylinder tests was chosen so that a sufficient amount of ice for measuring the ice amount and the cylinder diameter was collected. The relative increase in the cylinder diameter was low so that the time-dependence in the experiments was rather small. The model simulations were run using the time-step of one minute. The collection efficiency is calculated using the mean diameter of the cylinder during the experiment.

All the experiments on the rotating cylinders were made in the dry growth conditions where the resulting ice was rime and no run-off from the cylinder took place. However, at the beginning of the icing a nucleation delay of 0.5 - 2 minutes was observed.

Photographs of the ice accretions on cylinders of various diameters are shown in Fig. 8. Fig. 8 shows that the ice surface was generally quite smooth. At lower air temperatures, however, clearly visible roughness elements started to form on the surface [compare Figs. 8 and 9].

The mean collection efficiency based on the measured ice amounts at the air temperature of -5°C is plotted against the collection efficiency predicted by the theory in Fig. 10. These collection efficiencies were calculated using the mean diameter of the experimental ice deposit. Fig. 10 shows excellent agreement between the experimental results and the theory. In the mean, the relationship between the experimental E and the theoretical E is almost a direct proportionality, and the linear correlation coefficient between the two collection efficiencies is 0.98. Thus, the present model formulation of the dry growth process and the basic theory of the collection efficiency of cloud droplets presented in References 27 and 16 are quantitatively verified. Experimental relationships between the test conditions and the collection efficiency (or ice mass) are practically the same as those predicted by the theory and presented as figures by Makkonen [Refs. 28 and 8]. Here, only examples of the dependence of the collection efficiency on the cylinder diameter are shown in Fig. 11 to demonstrate the importance of time dependence in typical wire icing conditions, under which the cylinder size increases with time.

4.1.2 Ice density

The ice densities based on the measured ice amount and ice thickness as well as the ice densities predicted by the model are given in Table 1. The dependence of the ice density ρ on the

cylinder diameter D is shown in Fig. 12, and on air temperature t_a in Fig. 13. Figs. 12 and 13 demonstrate that the model assumption of the second order time-dependent effect, that ρ decreases as D increases in constant atmospheric conditions, is qualitatively correct. Qualitatively, the effects of the atmospheric parameters on ρ are also in accordance with the theory.

Fig. 12 points out that ρ is insensitive to the changes in the atmospheric parameters when D is very small. This justifies the use of constant density in the single rotating cylinder method of liquid water content [Ref. 20] and explains why Rogers et al. [Ref. 29] found no correlation between ρ and t_a on their LWC instrument based on measuring the rime rate.

A quantitative comparison between the observed and modeled ice densities [Table 1] shows that the model predictions of ρ are generally lower than the observed ρ. The reason for this is obvious in the light of the comparison between the droplet size measurement methods in Fig. 4, because Eq. (12) is based on Macklin's [Ref. 17] experiments in which the oil slide method was used in determining the median volume droplet diameter d_m. In the experiments by Macklin [Ref. 17] the range of the measured d_m was from 22 μm to 65 μm, but Fig. 4 suggests that the actual values of d_m have been considerably lower. That the discrepancy between the obseved and modeled densities may be explained by the error in the median volume diameter when determining Eq. (12) was verified by "correcting" the d_m values by Eq. (16) and running the model results with these "oil slide median volume diameters". This resulted in a much better agreement between the observed ρ and the modeled ρ, particularly at lower densities.

It is desirable in the icing modeling to have a parametrization of the ice density which is based on the true droplet size and to avoid the above-mentioned "correction" of the input d_m. Therefore, the ice density from our experiments was plotted against Macklin's ice density parameter R in Fig. 14. Fig. 14 includes also the previous model parametrization (dashed curve). The best fit equation describing the relationship between ρ(g cm^{-3} and R is

$$\rho = 0.378 + 0.425\ (\log R) - 0.0823\ (\log R)^2 \qquad (18)$$

Eq. (18) is proposed for future modeling at the values of R from 0.2 to 170 instead of Eq. (12).

4.2 The Wires

The test conditions of the wire icing experiments as well as the experimental results and the model predictions are presented in Table 2. The ice density given in Table 2 is based on the modified density parametrization (Eq. 18). The angle of the rotation of the wire at the end of the experiment is also given in Table 2.

The mean rotation rate varied between 65 and 223°/h and was slower for the 4 cm wire than for the 1 cm wire. In the mean, the angle of rotation increased approximately linearly with time, but there were considerable deviations in a short time-scale: In some cases the rotation ceased for as long a time as 20 minutes, and, on the other hand, there were sometimes rapid rotations of more than 90°. These movements resulted in the ice deposit shape that often differed from the circular shape and was sometimes closer to the rectangular shape. In the long-run these changes in the shape were partly smoothed out, but the final ice deposit shapes were still somewhat non-circular [Figs. 15 and 16b]. The wind drag seemed to have an important effect on the rotation of the wire: On some occasions the wire unwound more than 90° when the wind speed was reduced at the end of the experiment.

The qualitative model prediction, that the density of rime decreases with time (with increasing cylinder diameter), was clearly observed in the wire experiments, too. This can be seen from the visual appearance of the ice deposits in Fig. 17. The measured ice densities on the wires are smaller than the model prediction by a factor of ≈0.8. This is obviously due to the fact that the ice surface on the wires was rougher, consisting of rime feathers (see Figs. 16 and 17), and this resulted in a smaller overall density. The formation of roughness elements which may cover voids was obviously favoured by an initially rough wire surface and the long duration of the wire icing experiments.

A quantitative comparison between the observed ice mass on the wire and the model prediction is given in Fig. 18. The agreement is excellent in the mean, and the model predicts the ice mass with an accuracy of better than 30% in all the test conditions. This result is surprisingly good considering the deviations from the circular shape and the inaccuracy in the ice density.

The result in Fig. 18 is very encouraging as far as the practical application of transmission line icing is concerned. The linear correlation coefficient between the modeled ice mass and the experimental ice mass is 0.99. However, it must be pointed out that the results are sensitive to the liquid water content and droplet size which are difficult to estimate in natural icing conditions. The rotation of the wire may also be quite different from that reported here, since in the natural conditions the turbulent wind causes variation in the wind drag resulting in angular oscillations of the wire. There are many other problems related to the practical applications of the theory that should be examined, such as the effect of the angle between the transmission line orientation and the wind vector on the ice accretion. Nevertheless, the good agreement between the wire icing experiments in the wind tunnel and the present model show that when the time-dependence of the icing process is taken into account, a simple assumption, that the ice deposit is a circular cylinder in the mean, can be used as a basis of the modeling of the icing process in dry growth. This indicates that a complicated modeling of the ice accretion shape on

a rotating wire [e.g. Ref. 7] is not required in practical estimation of ice loading on transmission lines. The ice shape predictions is, however, useful in calculating the wind loading on iced wires [Ref. 30].

5.0 WET GROWTH CORRELATIONS

The experiments described in this report were made in the dry growth conditions. Icing under the wet growth conditions is of great importance also, as far as precipitation icing on transmission lines and icing of ships, as examples, are concerned. Therefore, some verifications of the theoretical model based on existing experimental data, are presented in this connection.

During recent years, the Mt. Washington Observatory and U.S. Army Cold Regions Research & Engineering Laboratory have measured wind and ice loads on a wire so as to simulate a section of a transmission line. These measurements were made on the top of Mt. Washington, NH, U.S.A. The wind and ice loads were recorded using a tri-axis load cell, and the meteorological observations are also available.

A set of data from these measurements was published in Reference 31 and can be compared with the theoretical model. Unfortunately, there is no simultaneous data on the liquid water content and droplet size for these measurements. However, it should be pointed out that in wet growth (clear ice) the atmospheric icing rate is quite insensitive to the liquid water content and droplet size [Ref. 28], so that for this growth regime a quantitative comparison is possible. In dry growth these data give only qualitative information. Fig. 19 shows the time-evolution of the vertical load in the data of Reference 31, and Fig. 20 the wind speed and air temperature for this icing event. The model simulation in Fig. 19 is shown as a solid line for wet growth and as broken lines after the point at which the model shows dry growth, respectively. The broken lines are examples of the dry growth simulations at various assumed droplet median volume diameters. A median volume diameter of 50 μm was assumed in the wet growth (freezing drizzle was reported at that time). The liquid water content of 0.5 gm^{-3} assumed in the model simulation is the estimated mean value of LWC at Mt. Washington in icing conditions [Ref. 32]. The observed clear ice deposits were reported to be relatively smooth [Ref. 31], and the equivalent sand grain roughness of 1 mm was assumed in the model calculations.

Fig. 19 shows that qualitatively the observed time-evaluation of the ice load is similar to the model prediction in that the growth rate of the ice load increases in wet growth and decreases in dry growth. The model also predicts the transition from wet to dry growth. Changing the assumed liquid water content, median volume droplet diameter or roughness within reasonable limits would not change the modeled growth rate of glaze ice load

by more than ≈30%. Hence Fig. 19 indicates that the model gives useful estimates of the ice loads formed under wet growth conditions in the natural environment.

Another verification of the wet growth theory can be made by comparing its results with the cylinder icing wind tunnel measurements by Stallabrass and Hearty [Ref. 33]. In these experiments sea spray was simulated, so that the liquid water content was 3.2 gm^{-3} and median volume droplet diameter 200 μm resulting in wet growth at all test temperatures (-15°C to -4.5°C). Wind speed was constant at 22.4 ms^{-1}, and four cylinders of diameters varying from 3.8 cm to 45.7 cm were tested in both horizontal and vertical position. Test duration was one hour.

In the experiments in Ref. 33, the cylinders were fixed. This requires a modification of the model, which assumes a slowly rotating cylinder, so that comparable model predictions can be made. The original model version distributes the accreted ice evenly around the cylinder (Eq. 4). For the purpose of the comparison with the data of Ref. 33, the ice is distributed in the model on the windward side of the cylinder only, as shown in Fig. 21. Based on the photographs and drawings of the ice accretions, it was estimated that the height of the roughness elements was ≈3 mm in the mean. This value was then used in the model.

The result of the comparison is given in Fig. 22 and shows a strong linear correlation between the experimental results and the model prediction ($r = 0.97$). The modeled ice loads are ≈2 kg m^{-1} smaller than the experimental ice loads in the mean. This is probably caused by the fact that the actual ice deposit had usually a larger surface area for the heat transfer to take place than the model ice deposit (c.f. Fig. 21). Generally speaking, however, the shape of the ice deposit seems to have a remarkably small effect on the rate of icing, as shown by the fact that the model simulates the icing rate on horizontal and vertical cylinders almost equally well. This is encouraging considering practical applications in which the shape of the ice accretion is not known.

6.0 CONCLUSIONS

The main conclusions from the laboratory experiments presented in this report and the comparisons between the previous empirical results and the time-dependent icing model are as follows:

- The traditionally used oil slide method of droplet size measurement overestimates the median volume droplet diameter d_m in the typical range of d_m of atmospheric icing conditions. This has, in previous studies, resulted in empirical relationships between the atmospheric conditions and the density of accreting ice, as an example, that give erroneous results if the true droplet size is used.

- Applying the theory of the collection efficiency of cloud droplets on a smooth circular cylinder in time-dependent icing model results in an excellent agreement with the icing experiments on evenly rotating cylinders.

- The time-dependent numerical model of the rate of rime formation based on the assumption of a circular object shape is applicable to the simulated transmission line rime icing in spite of the variations in the ice deposit shape and roughness of the surface.

- The rime density on circular evenly rotating cylinders can be modeled using the Macklin density parameter with a good accuracy. On transmission line cables the ice density seems to be typically 20% lower than the model prediction because of the formation of voids of a much larger scale than the size of the impacting droplets.

- The overall icing rate in the wet growth regime is relatively insensitive to the shape of the ice deposit, and useful predictions of the rate of glaze formation on cylinders and wires can be made with the icing model.

7.0 REFERENCES

1. Bendel, W.B.
   Paton, D.
   "A review on the effect of ice storms on the power industry".
   Journal of Applied Meteorology, Vol. 20, 1981, pp.1445-1449.

2. Imai, I.
   "Studies of ice accretion".
   Research on Snow and Ice, Vol. 1, 1953, pp.35-44 (in Japanese).

3. Diem, M.
   "Ice loads on high voltage conductors in the mountains".
   Archives for Meteorology, Geophysics and Bioclimatology, Ser. B, Vol. 7, 1956, pp.84-95 (in German).

4. Kuroiwa, D.
   "Icing and snow accretion on electric wires"
   U.S. Army Cold Regions Research and Engineering Laboratory, Report No. 123, 1965, 10 pp.

5. Poots, G.
   Rodgers, G. G.
   "The icing of a cable".
   Journal of the Institute of Mathematics and its Applications, Vol. 18, 1976, pp.203-217.

6. Zavarian, M.V.
Glukhov, V.G.
Mytarev, M.N.
"A method for the calculation of ice loads on high constructions".
Zeitschrift fur Meteorologie, Vol. 26, 1976, pp.98-104 (in German).

7. McComber, P.
"Numerical simulation of cable twisting due to icing".
Cold Regions Science and Technology, Vol. 8, 1984, pp.253-259.

8. Makkonen, L.
"Modeling of ice accretion on wires".
Journal of Climate and Applied Meteorology, Vol. 23, 1984 (in press).

9. McComber, P.
Touzot, G.
"Calculation of the impingement of cloud droplets on a cylinder by the finite element method".
Journal of the Atmospheric Sciences, Vol. 38, 1981, pp.1027-1036.

10. Smith, M. E.
Arimilli, R.V.
Keshock, E.G.
"Measurement of local convective heat transfer coefficient of four ice accretion shapes".
Department of Mechanical and Aerospace Engineering, University of Tennessee Technical Report, Part I, 1983, 95 pp.

11. Makkonen, L.
"Heat transfer and icing of a rough cylinder".
Cold Regions Science and Technology, Vol. 8, 1984 (in press).

12. Langmuir, I.
"Super-cooled water droplets in rising currents of cold saturated air".
The collected works of Irving Langmuir, Pergamon Press, Vol. 10, 1961, pp.199-334.

13. Brun, R.J.
Lewis, W.
Perkins, P.J.
Serafini, J.S.
"Impingement of cloud droplets on a cylinder and procedure for measuring liquid-water content and droplet sizes in supercooled clouds by rotating multicylinder method".
Lewis Flight Propulsion Laboratory, Cleveland, Ohio, Report No. 1215, 1955, 43 pp.

14. Dranevic, E.P.
"Glaze and Rime".
Gidrometeorologitseskoii Izdatelstvo, Leningrad, 1971, 227 pp. (in Russian).

15. Howe, J.B.
"Measurement and analysis of icing and wind loads on wires".
Unpublished report prepared for U.S. Army Cold Regions Research and Engineering Laboratory, 1982, 8 pp.

16. Langmuir, I.
Blodgett, K.B.
"A mathematical investigation of water droplet trajectories".
U.S.A. Air Force Technical Report No. 5418, 1946, 65 pp. (reprinted in: The collected works of Irving Langmuir, Pergamon Press, Vol. 10, 1961, pp. 335-393).

17. Macklin, W.C.
"The density and structure of ice formed by accretion".
Quarterly Journal of Royal Meteorological Society, Vol. 88, 1962, pp.30-50.

18. Bain, M.
Gayet, J.F.
"Contribution to the modeling of the ice accretion process: Ice density variation with the impact surface angle".
Annals of Glaciology, Vol. 4, 1982, pp.19-23.

19. Lozowski, E.P.
Stallabrass, J.R.
Hearty, P.F.
"The icing of an unheated nonrotating cylinder. Part II: Icing wind tunnel experiments".
Journal of Climate and Applied Meteorology, Vol. 22, 1983, pp.2063-2074.

20. Stallabrass, J.R.
"An appraisal of the single rotating cylinder method of liquid water content measurement".
National Research Council of Canada Report LTR-LT-92, 1978, 21 pp.

21. Golitzine, N.
"Method for measuring the size of water droplets in clouds, fogs and sprays".
National Research Council of Canada Report ME-177, 1950, 13 pp.

22. Gall, E.S.
Floyd, F.X.
"Icing test capability of the engine test facility propulsion development test cell (J-1)".
U.S.A.F., Arnold Engine Development Center Report AEDC-TR-71-94, 1971, 42 pp.

23. Keller, R.G.
"Measurement and control of simulated environmental icing conditions in an outdoor, free jet, engine ground test facility".
NATO, AGARD-CP-236, 1978, pp.7-1 - 7-13.

24. Gates, E.M.
"Measurement of water droplet distributions in an icing wind tunnel by holography".
Proceedings of First International Workshop on Atmospheric Icing of Structures, U.S. Army Cold Regions Research and Engineering Laboratory, Special Report 83-17, 1983, pp.3-11.

25. Dye, J.E.
Baumgardner, D.
"Electronic and optical studies of the FSSP".
Submitted to Atmospheric and Oceanic Technology.

26. Lee, J.D.
Gregorek, G.M.
"Performance of two transonic airfoil wind tunnels utilizing limited ventilation".
Proceedings of the Wind Tunnel Wall Interference Assessment/Correction Workshop, NASA Langley Research Center, 1983.

27. Albrecht, F.
"Teoretische Untersuchungen uber die Ablagerung von Staub aus stromender Luft und ihre Anwendung auf die Theorie der Staubfilter".
Physikalische Zeitschrift, Vol. 32, 1931, pp.48-56.

28. Makkonen, L.
"Estimating intensity of atmospheric ice accretion on stationary structures"
Journal of Applied Meteorology, Vol. 20, 1981, pp.595-600.

29. Rogers, D.C.
Baumgardner, D.
Vali, G.
"Determination of supercooled liquid water content by measuring rime rate".
Journal of Climate and Applied Meteorology, Vol. 22, 1983, pp.153-162.

30. McComber, P.
Morin, G.
Martin, R.
Van, L.V.
"Estimation of combined ice and wind load on overhead transmission lines".
Cold Regions Science and Technology, Vol. 6, 1983, pp.195-206.

31. Govoni, J.W.
Ackley, S.F.
"Field measurements of combined icing and wind loads on wires".
Proceedings of First International Workshop on Atmospheric Icing of Structures, U.S. Army Cold Regions Research and Engineering Laboratory Special Report 83-17, 1983, pp.205-213.

32. Howe, J.B.
"Tests of two Rosemount ice detectors at the Mt. Washington Observatory late winter 1982".
Unpublished report prepared for U.S. Army Cold Regions Research and Engineering Laboratory, 1982, 5 pp.

33. Stallabrass, J.R.
Hearty, P.F.
"The icing of cylinders in conditions of simulated freezing sea spray".
National Research Council of Canada Report MD-50, 1967, 15 pp.

34. Keppe, L. "Description of icing cases which led to tower collapse on 300 kV electric power line Dale-Fana".
Paper presented at 2nd International Workshop on Atmospheric Icing on Structures, Trondheim, Norway, June 1984.

Fig. 1 Cylindrical ice accretion on 300 kV power line, Dale-Fana, Norway
(Reproduced with permission from Ref. 34)

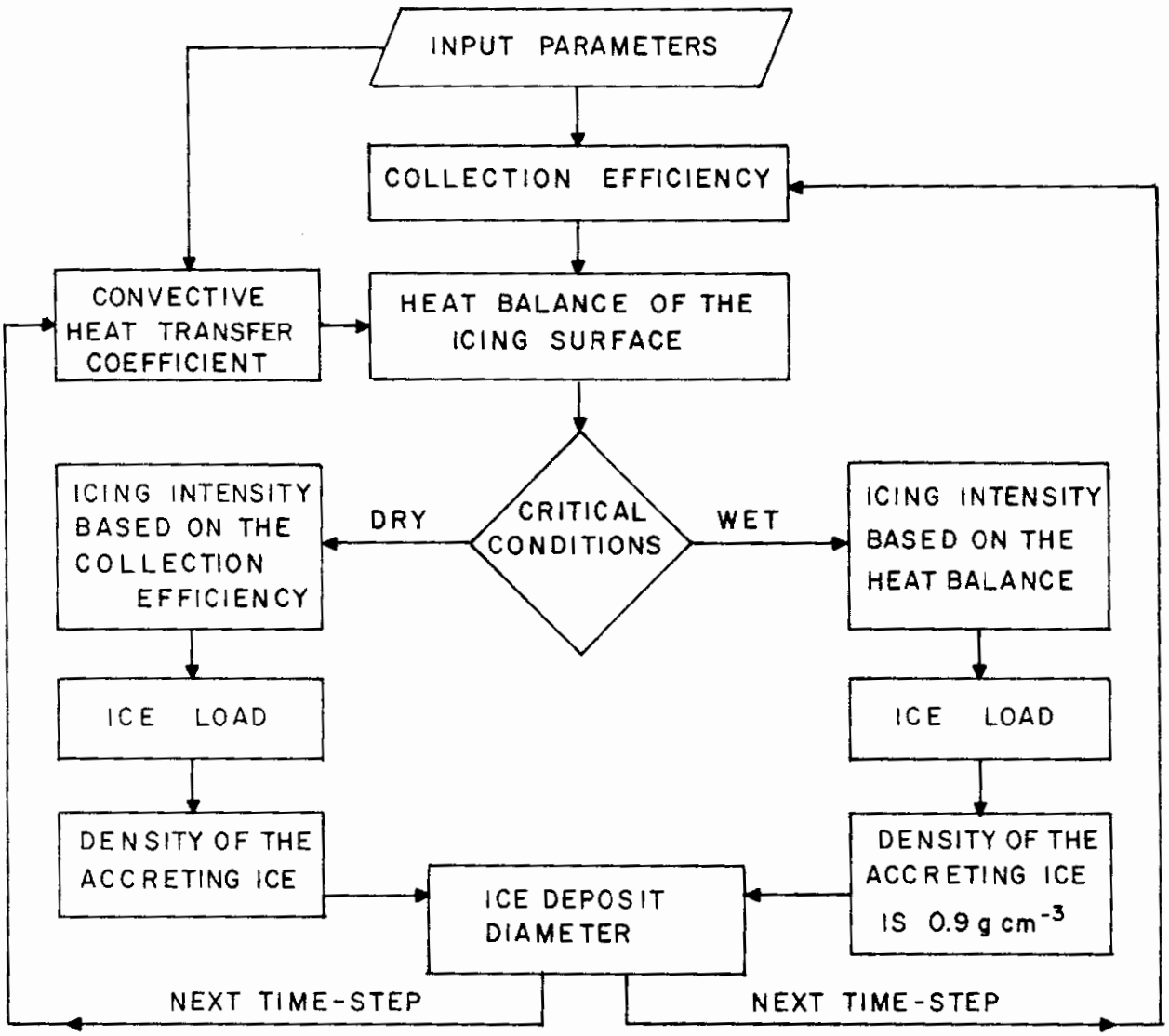

Fig. 2 Block diagram of the numerical icing model.

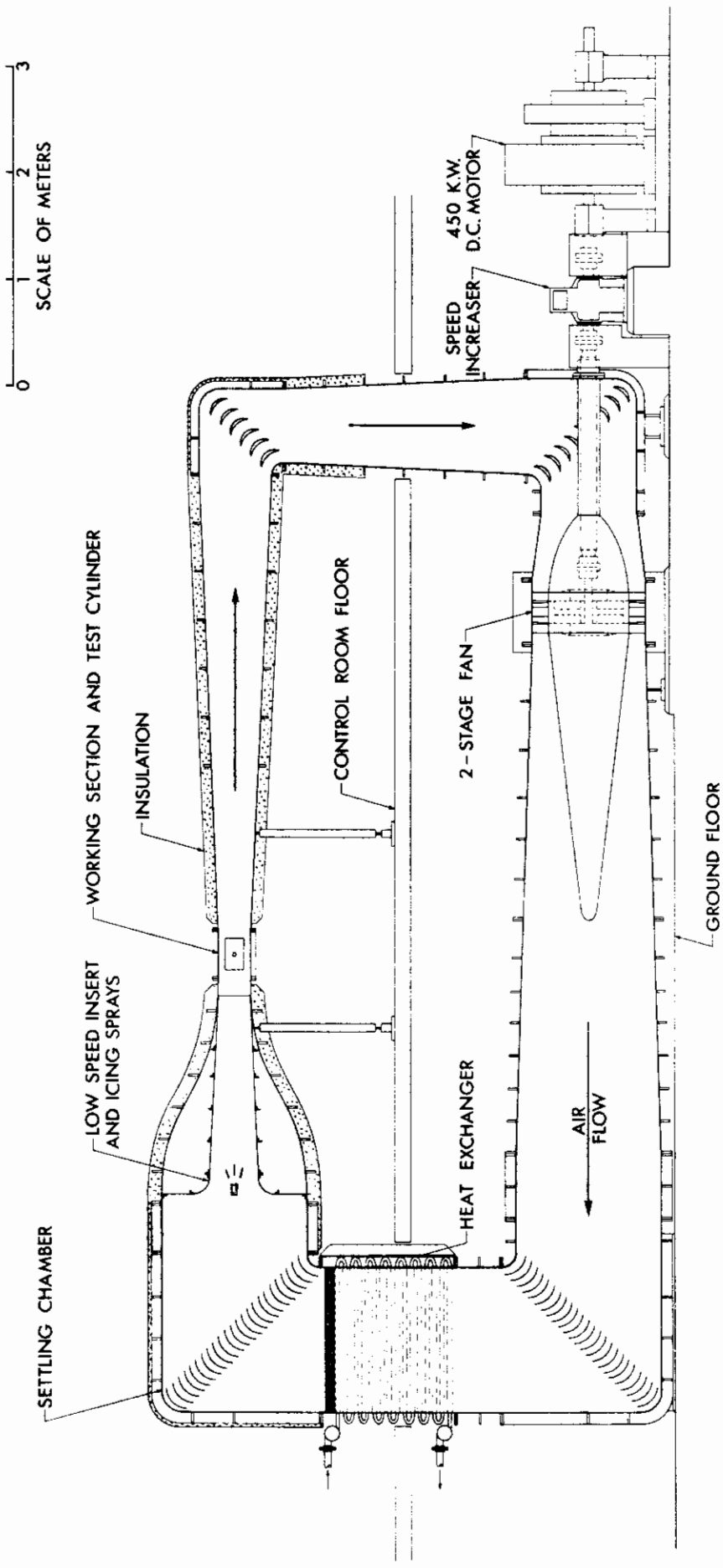

Fig. 3 National Research Council of Canada's icing wind tunnel.

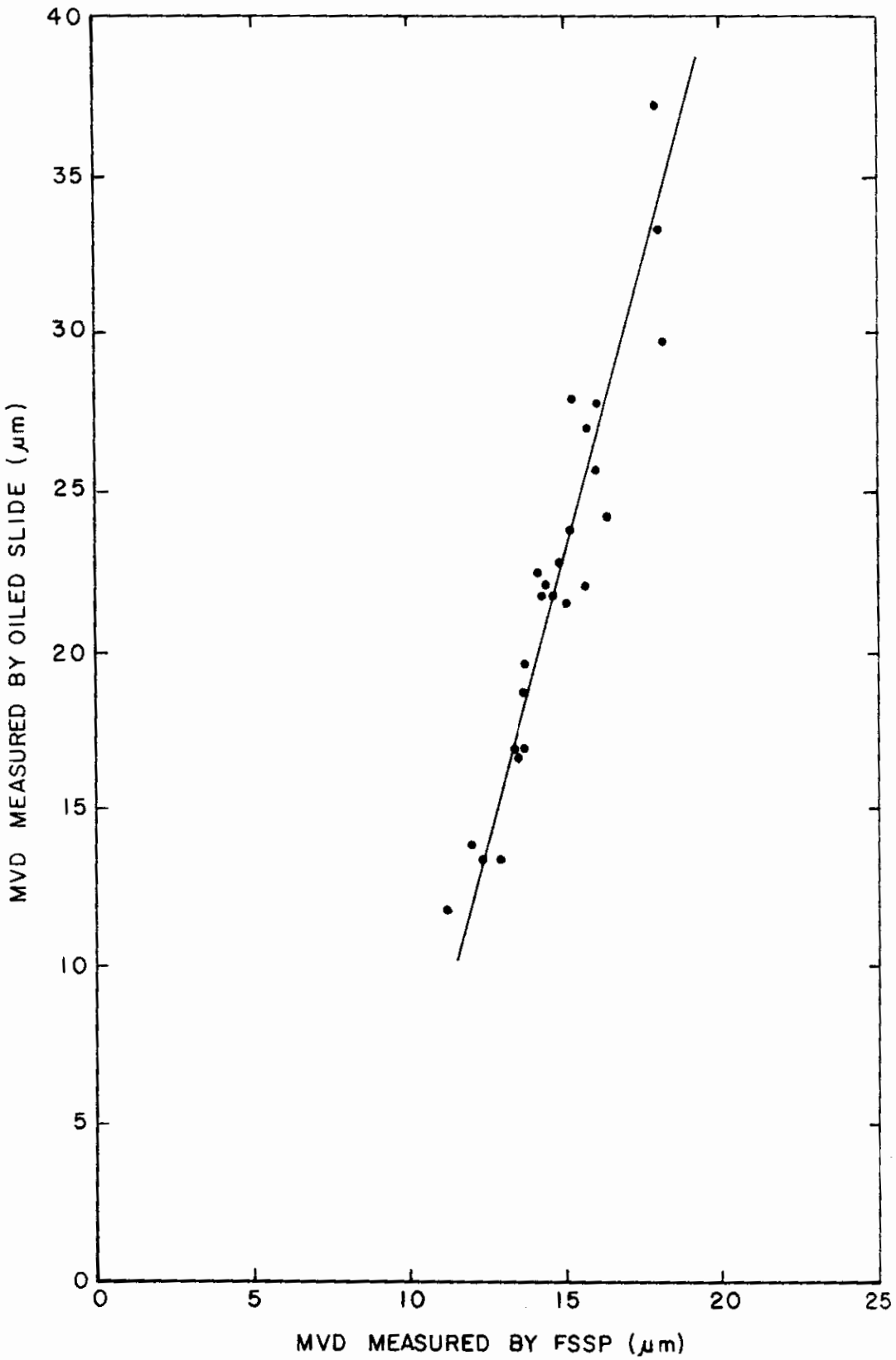

Fig. 4 Experimental relationship of droplet median volume diameters as measured by Oiled Slide and Forward Scattering Spectrometer Probe

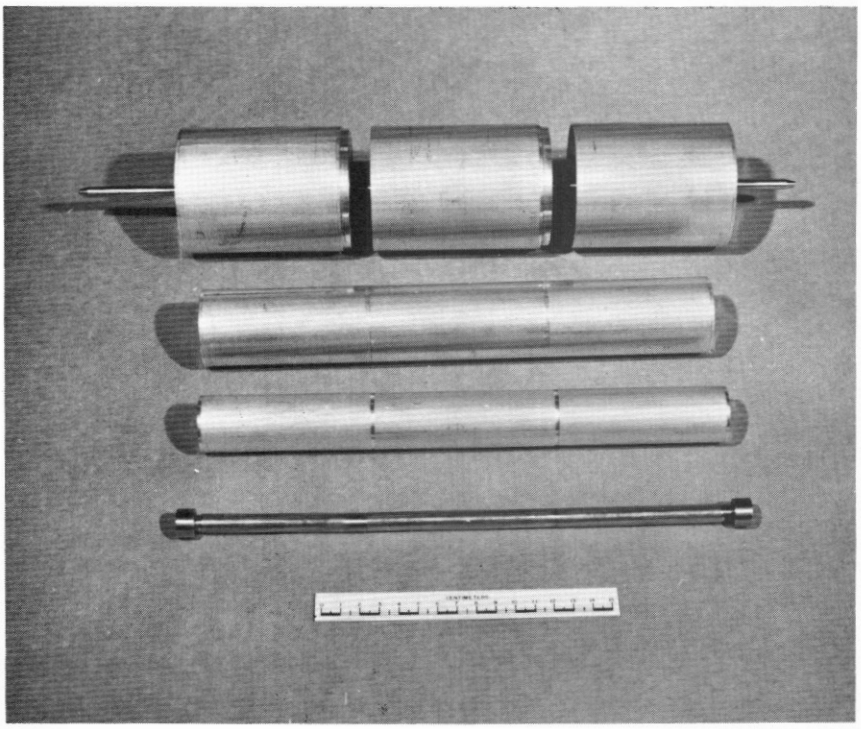

Fig. 5 The four rotating cylinders.

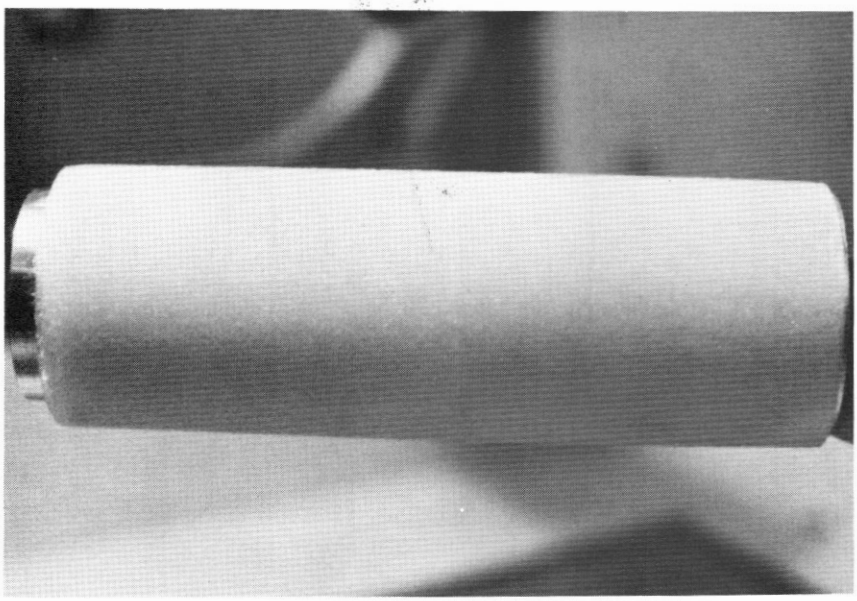

Fig. 6 Centre section of 3.183 cm diameter cylinder at end of Test 8, showing clean ice separation.

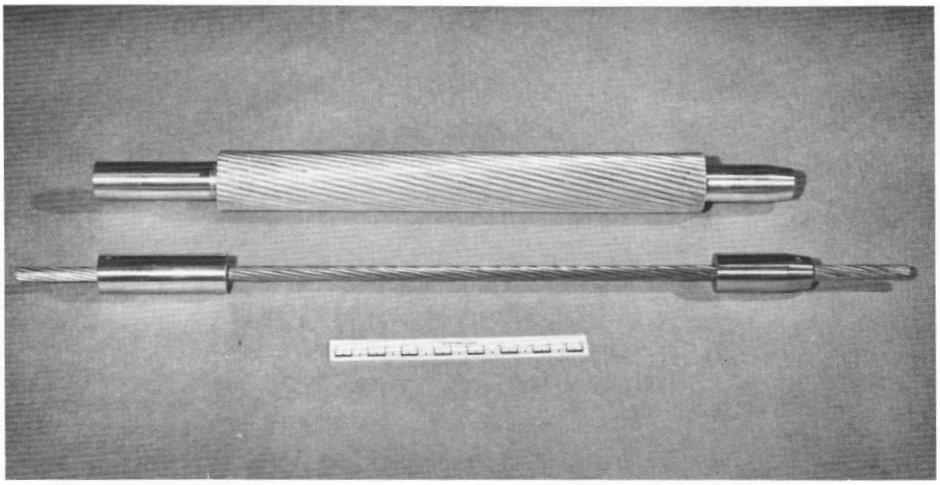

Fig. 7 The two simulated wires used in the wind tunnel tests.

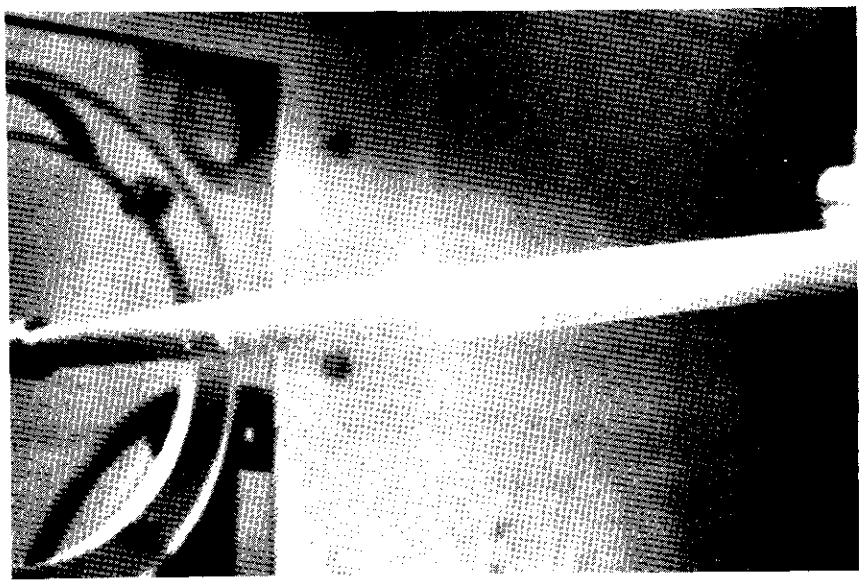

(a) 1.024 cm Diameter Cylinder. Test 4
Ice Density 0.87 g cm^{-3}

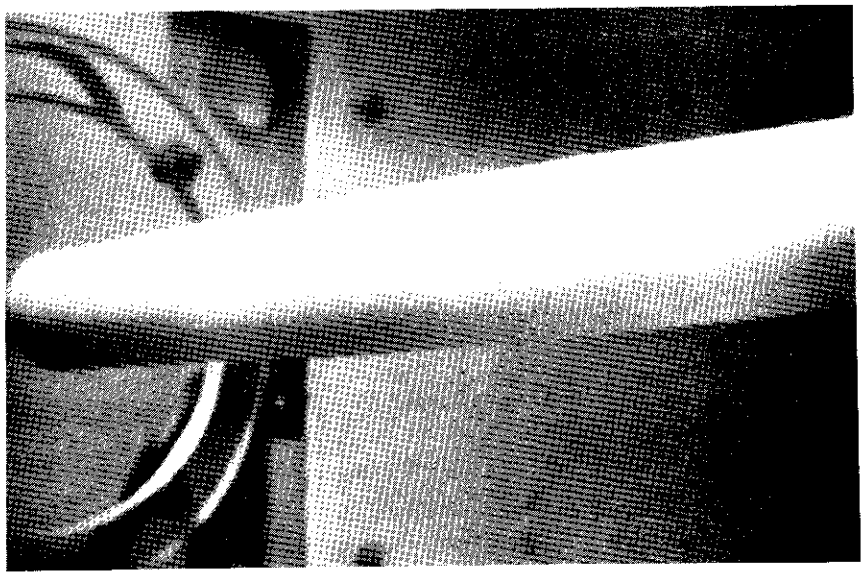

(b) 3.183 cm Diameter Cylinder. Test 9
Ice Density 0.83 g cm^{-3}

Fig. 8 Rotating Cylinder Icing

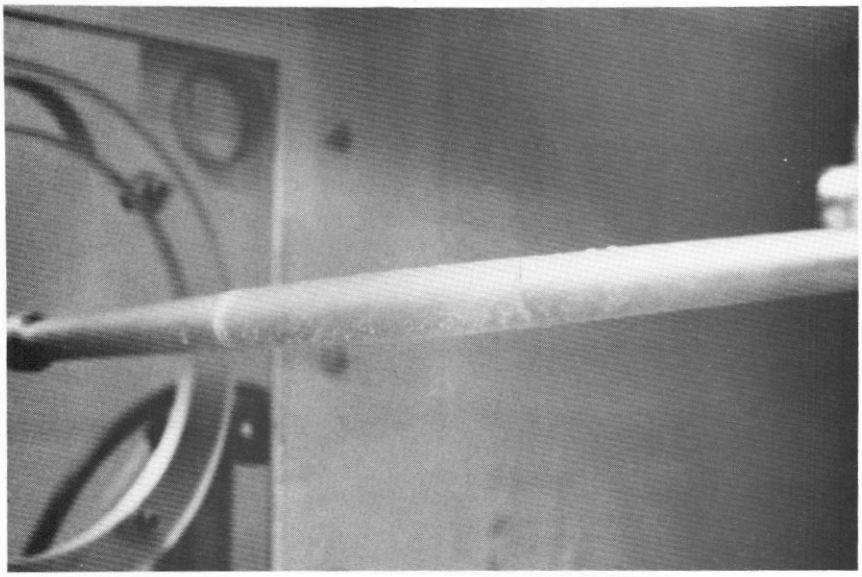

(a) 1.024 cm Diameter Cylinder. Test 4
Ice Density 0.87 g cm^{-3}

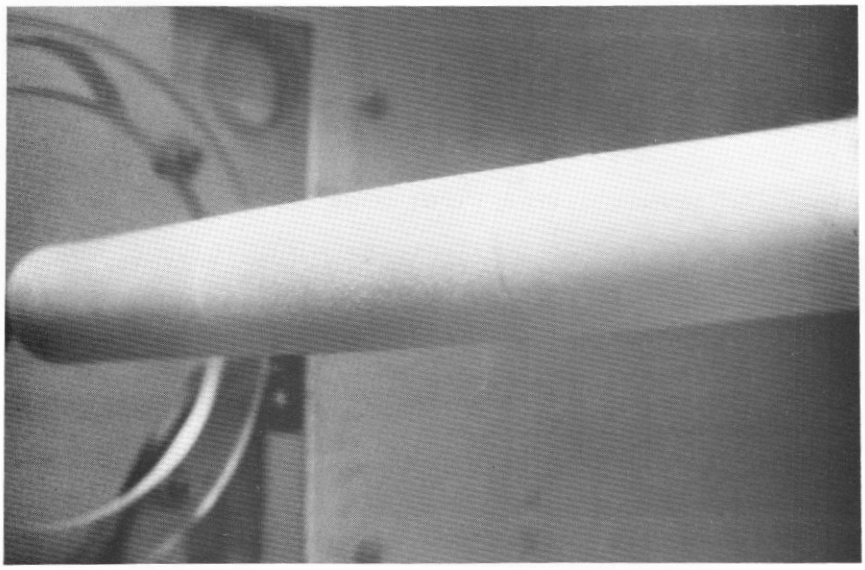

(b) 3.183 cm Diameter Cylinder. Test 9
Ice Density 0.83 g cm^{-3}

Fig. 8 Rotating Cylinder Icing

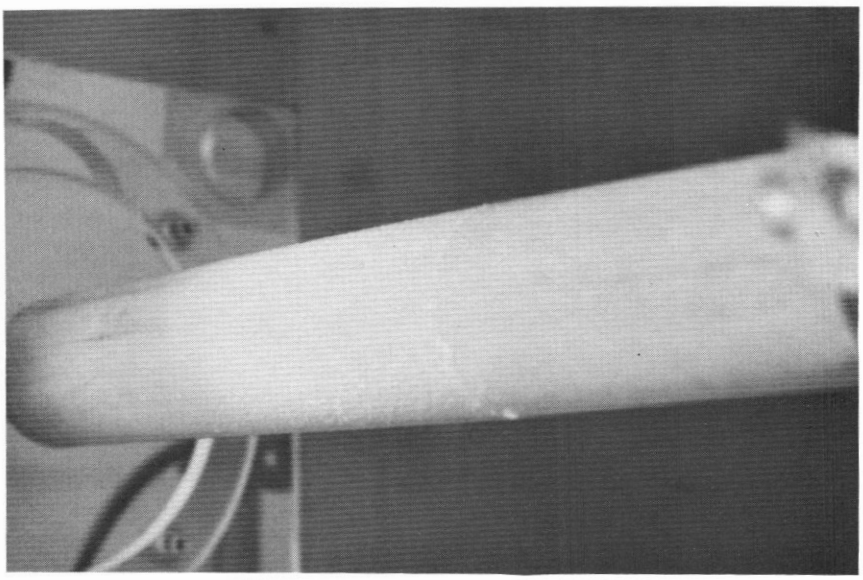

(c) 4.44 cm Diameter Cylinder. Test 19
Ice Density 0.63 g cm^{-3}

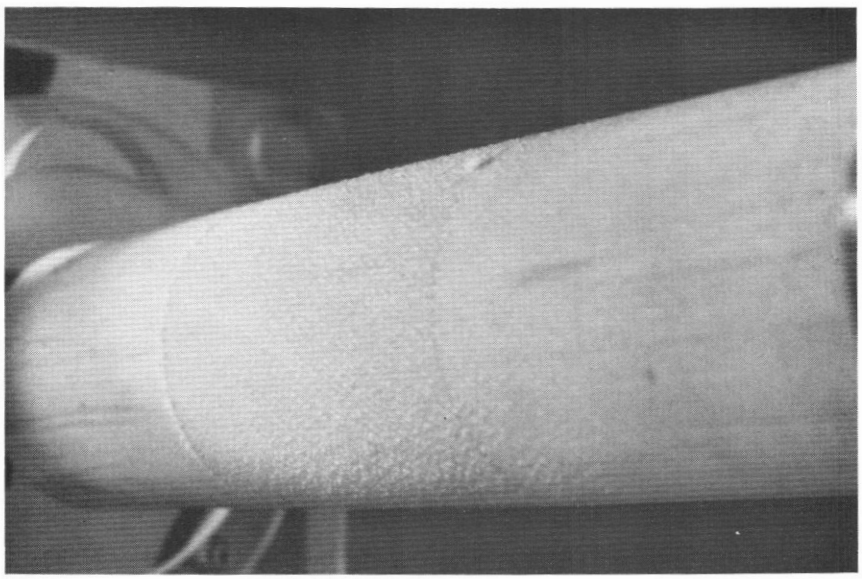

(d) 7.609 cm Diameter Cylinder. Test 24
Ice Density 0.46 g cm^{-3}

Fig. 8 cont. Rotating Cylinder Icing

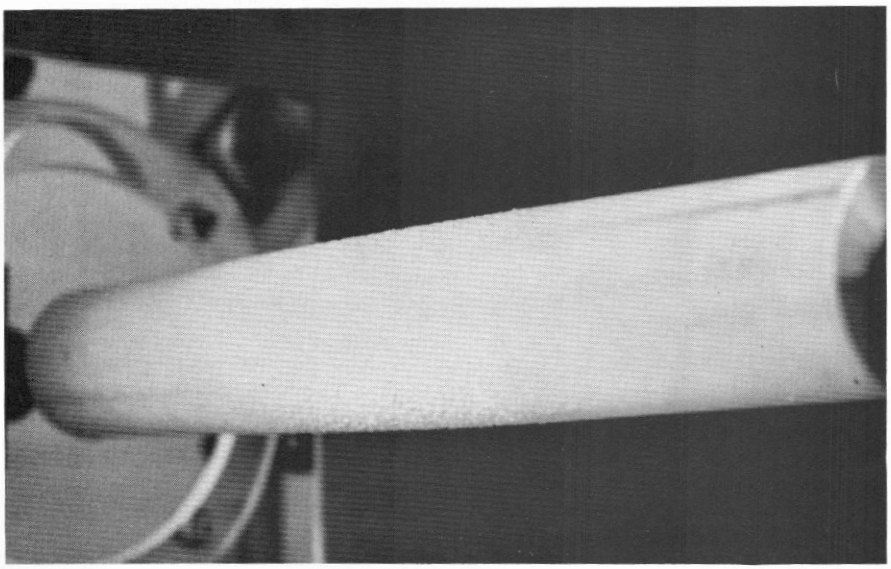

(a) Test 20E. Temperature -10°. Ice Density 0.61 g cm^{-3}

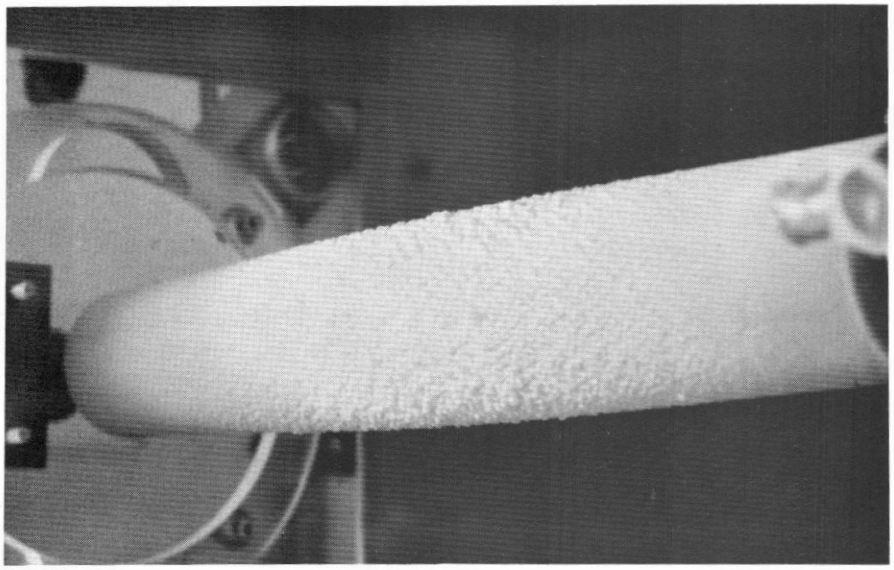

(b) Test 20F. Temperature -20°. Ice Density 0.42 g cm^{-3}

Fig. 9 Rotating Cylinder Icing - Effect of Temperature
4.44 cm Diameter Cylinder

MODEL COLLECTION EFFICIENCY

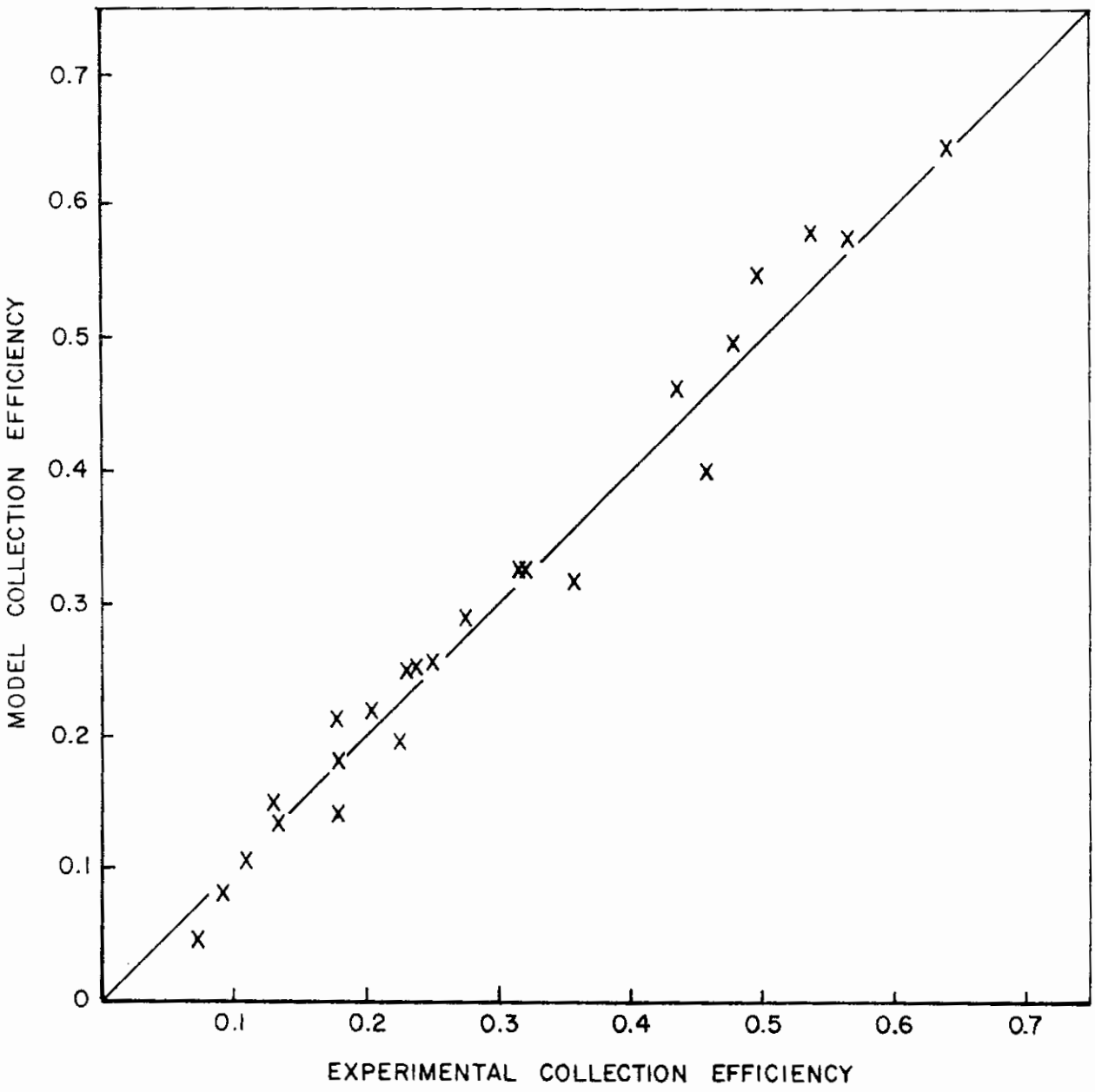

Fig. 10 Mean collection efficiency on rotating cylinders as predicted by the theory versus the experimental mean collection efficiency.

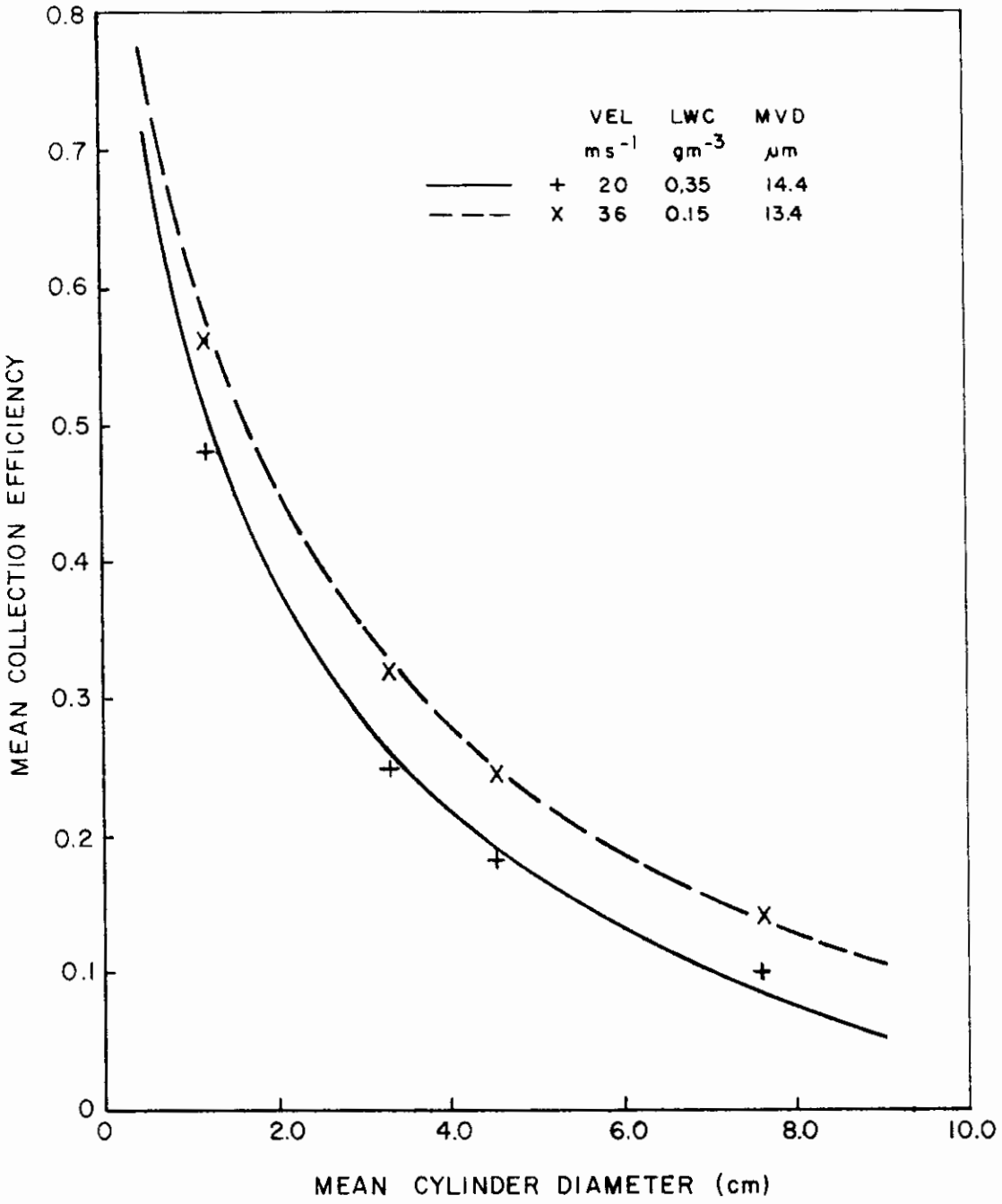

Fig. 11 Mean collection efficiency on a rotating circular cylinder under two sets of experimental conditions vs. the mean diameter of the cylinder during the experiment. Points are experimental values and the lines are the theoretical predictions.

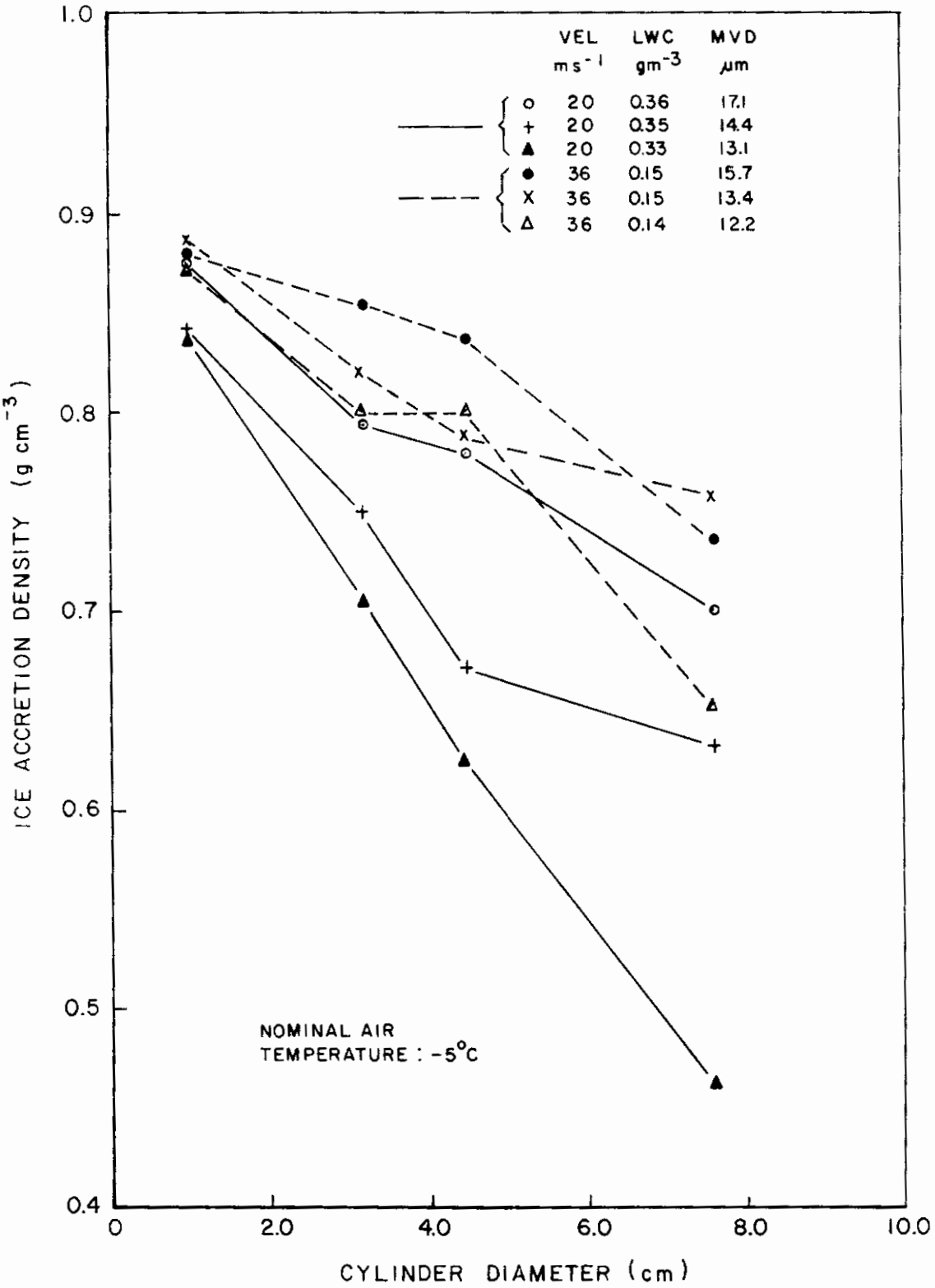

Fig. 12 Density of ice accretion as a function of initial cylinder diameter, for various experimental conditions.

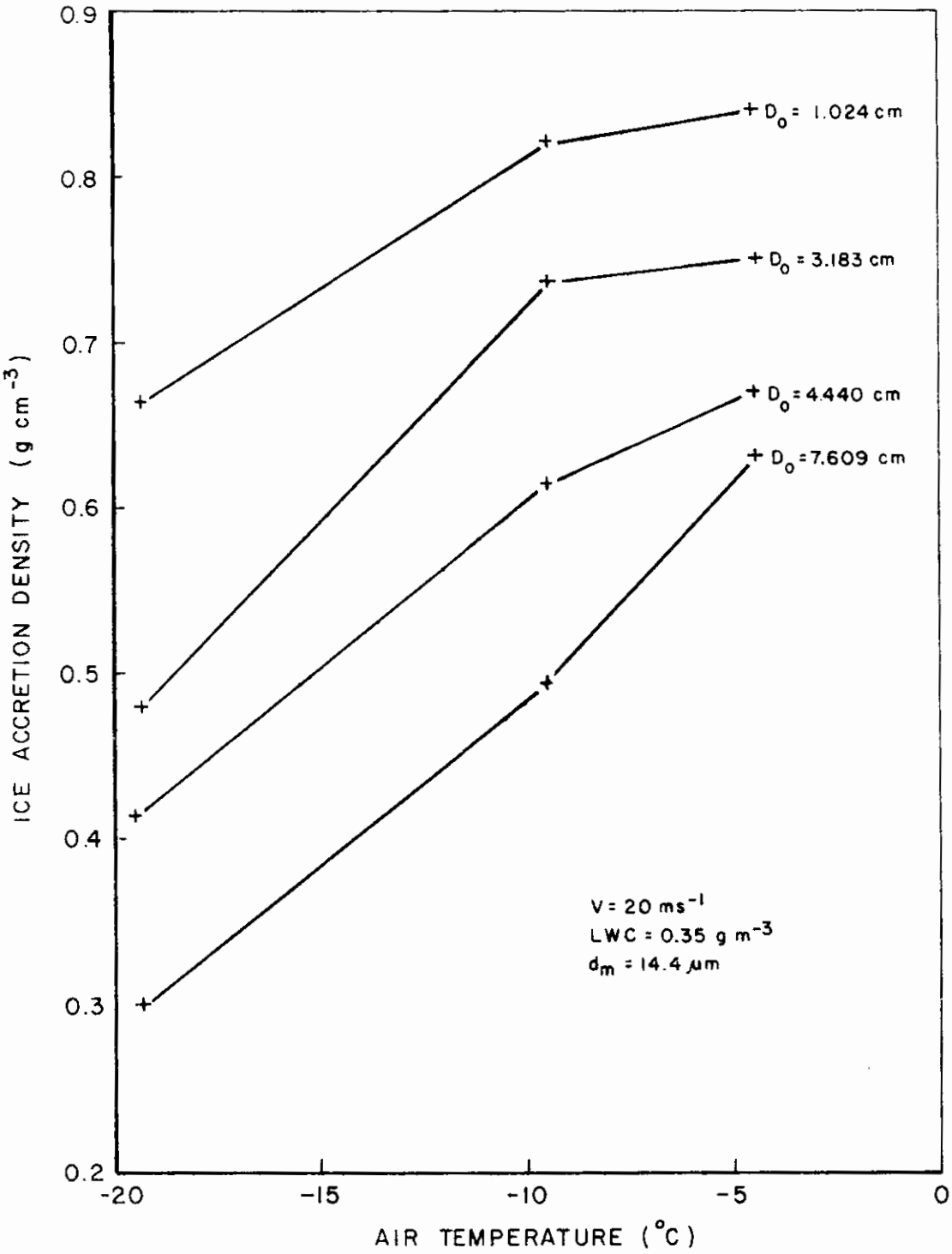

Fig. 13 Temperature dependence of ice accretion density -- experimental results.

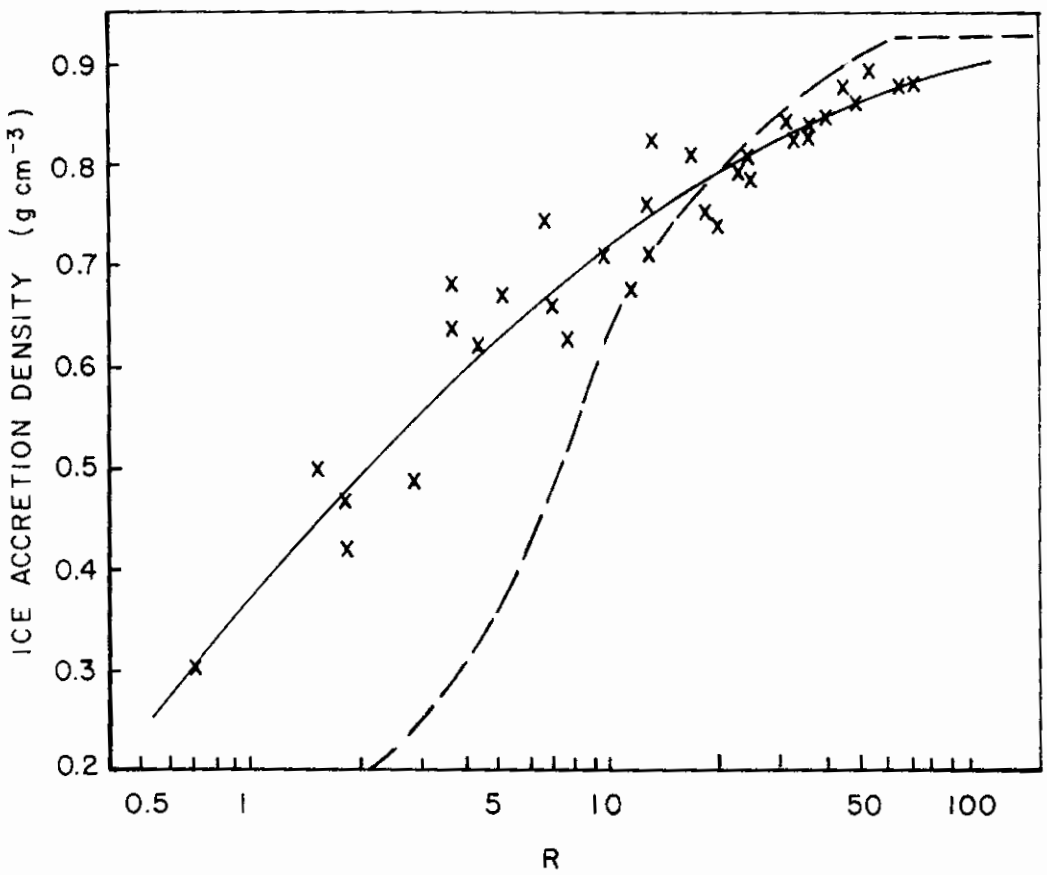

Fig. 14 Ice accretion density on the rotating cylinders vs. Macklin's density parameter R. Solid line is the best fit line [eq. (18)] and the broken line is the earlier model parameterization [eq. (12)].

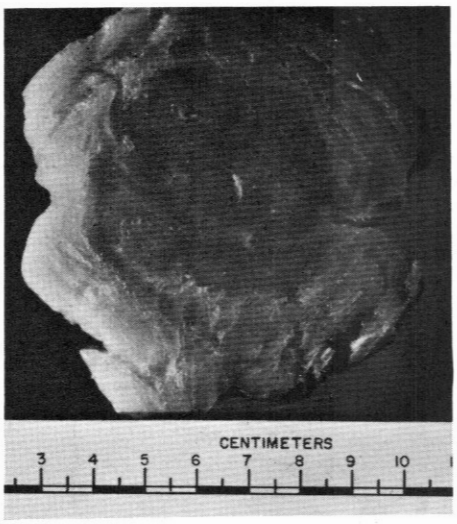

(a) Test W1 D = 1 cm
v = 30 m/s t_a= -4.7°C
w = 0.32 gm^{-3} d_m= 13.6 μm

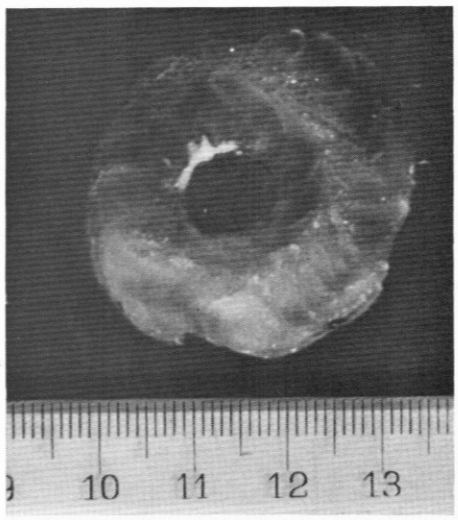

(b) Test W3 D = 1 cm
v = 20 m/s t_a= -4.5°C
w = 0.35 gm^{-3} d_m= 14.4 μm

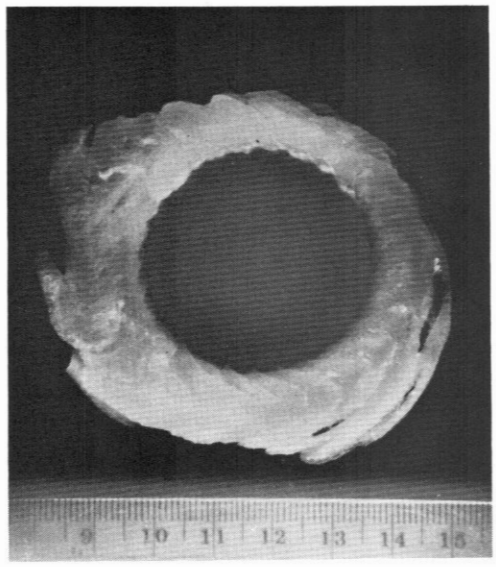

(c) Test W6 D = 4 cm
v = 30 m/s t_a= -4.3°C
w = 0.32 gm^{-3} d_m= 13.6 μm

Fig. 15 Cross-sections of Ice Accretions on Wires

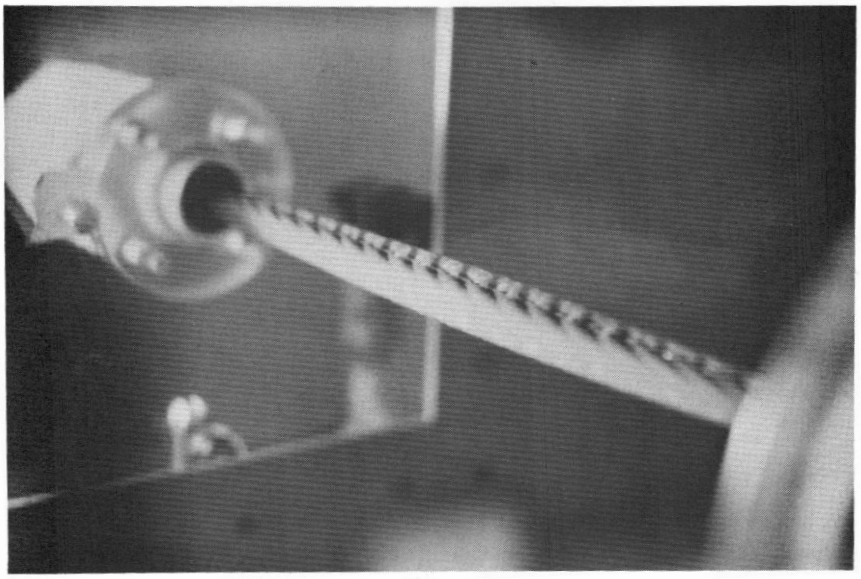

(a) Test W2 after 30 minutes. Wire rotation 210°.

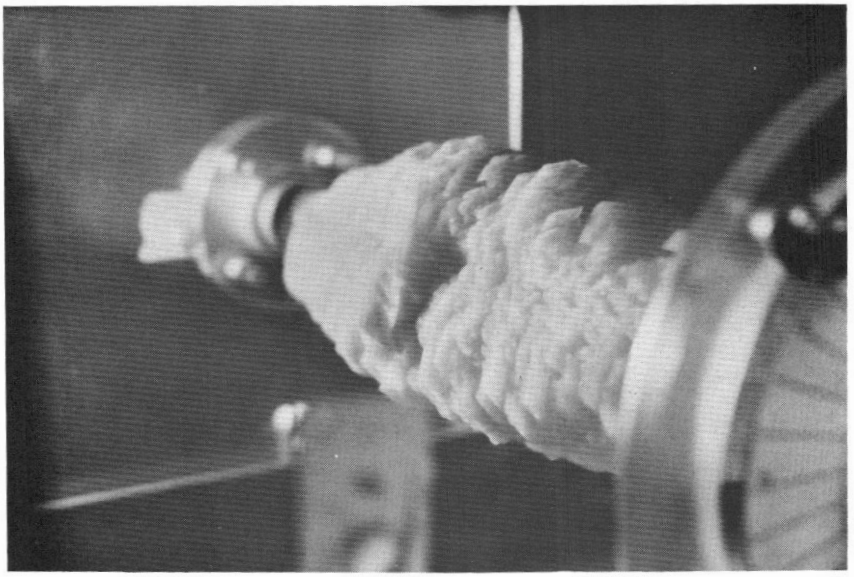

(b) Test W1 after 10 hours. 5 revolutions of wire.

Fig. 16 Examples of icing on 1 cm diameter wire.

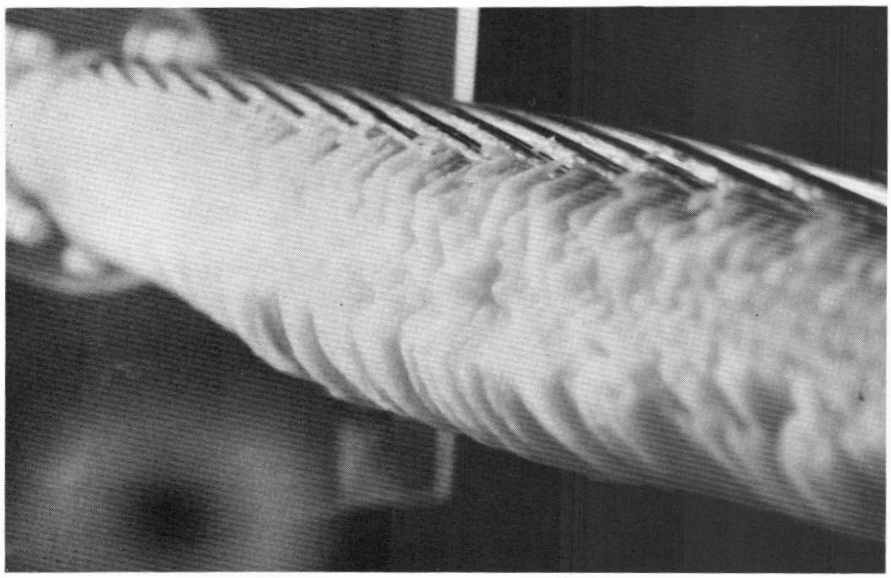

(a) Test W8 after 4 hours. Wire rotation 260°.

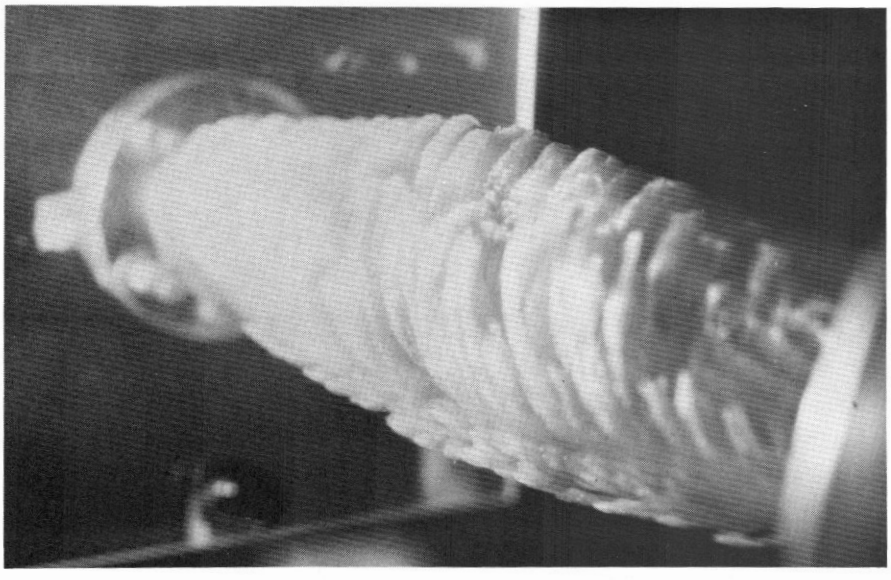

(b) Test W6 after 4 hours. Wire rotation 455°.

Fig. 17 Examples of icing on 4 cm diameter wire.

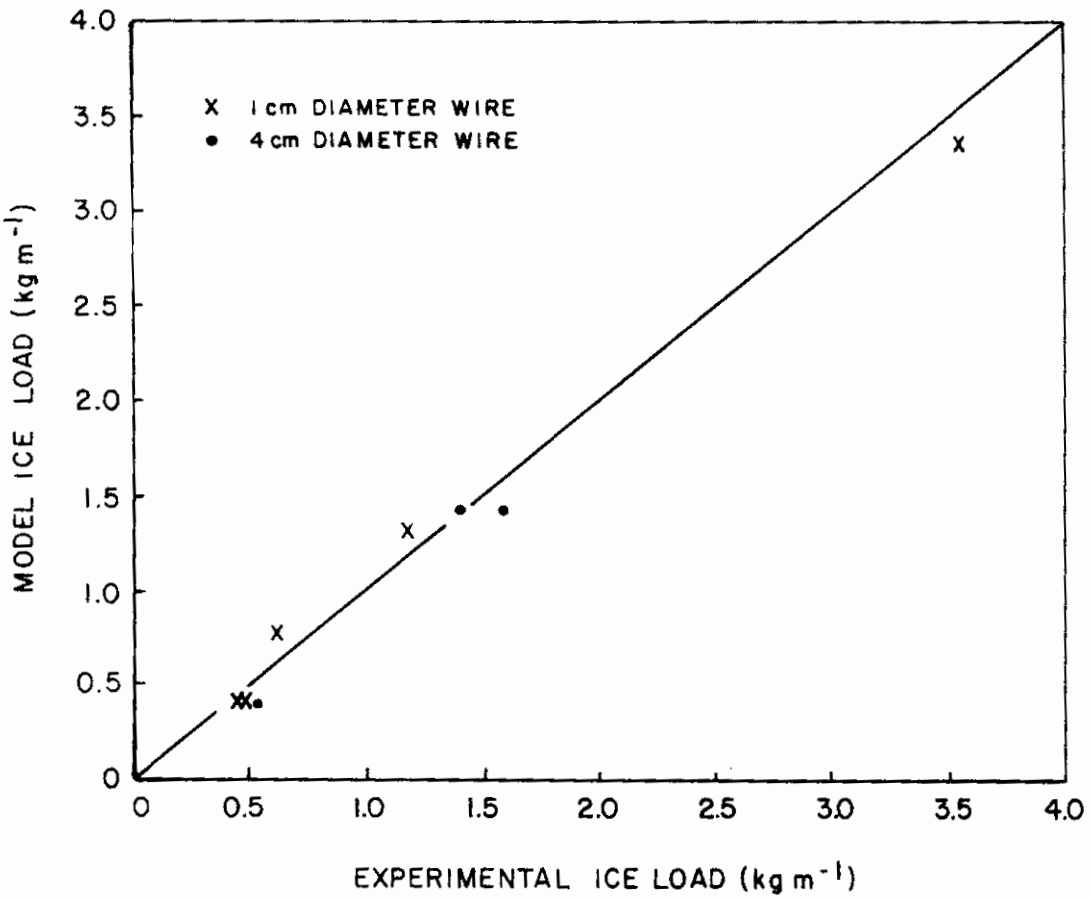

Fig. 18 Ice load predicted by the model vs. the experimental ice load in the wind tunnel tests simulating the icing of transmission line cables.

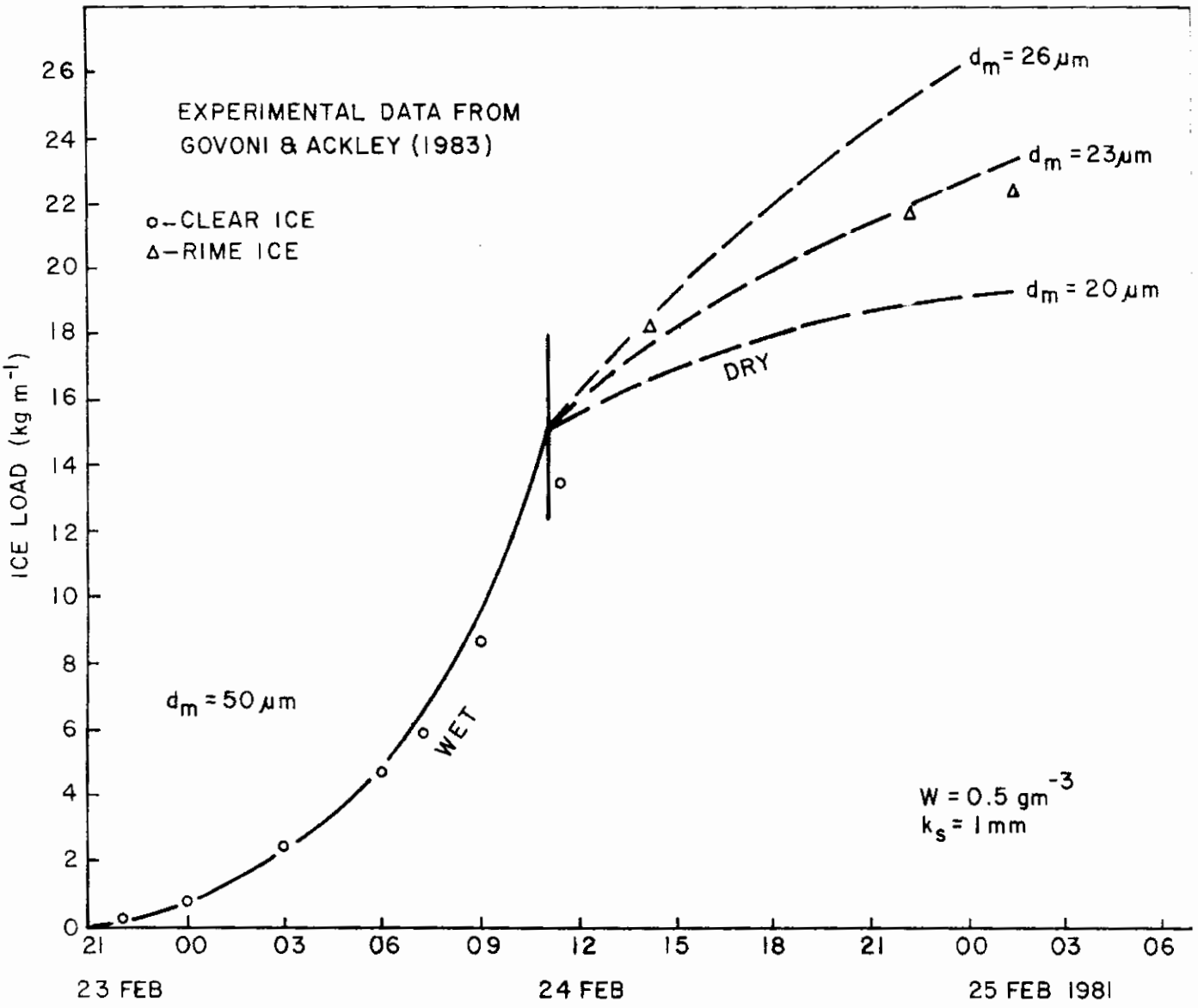

Fig. 19 Evolution of the ice load on a 0.6 cm diameter wire on Mt. Washington 23-25 February 1981. Points represent the observations and the solid line the model simulation for wet growth. The vertical line shows the modeled transition from wet to dry growth, and the broken lines are examples of model simulations in dry growth at various median volume droplet diameters. Experimental data from Reference 31. Air temperature and wind speed are given in Fig. 19.

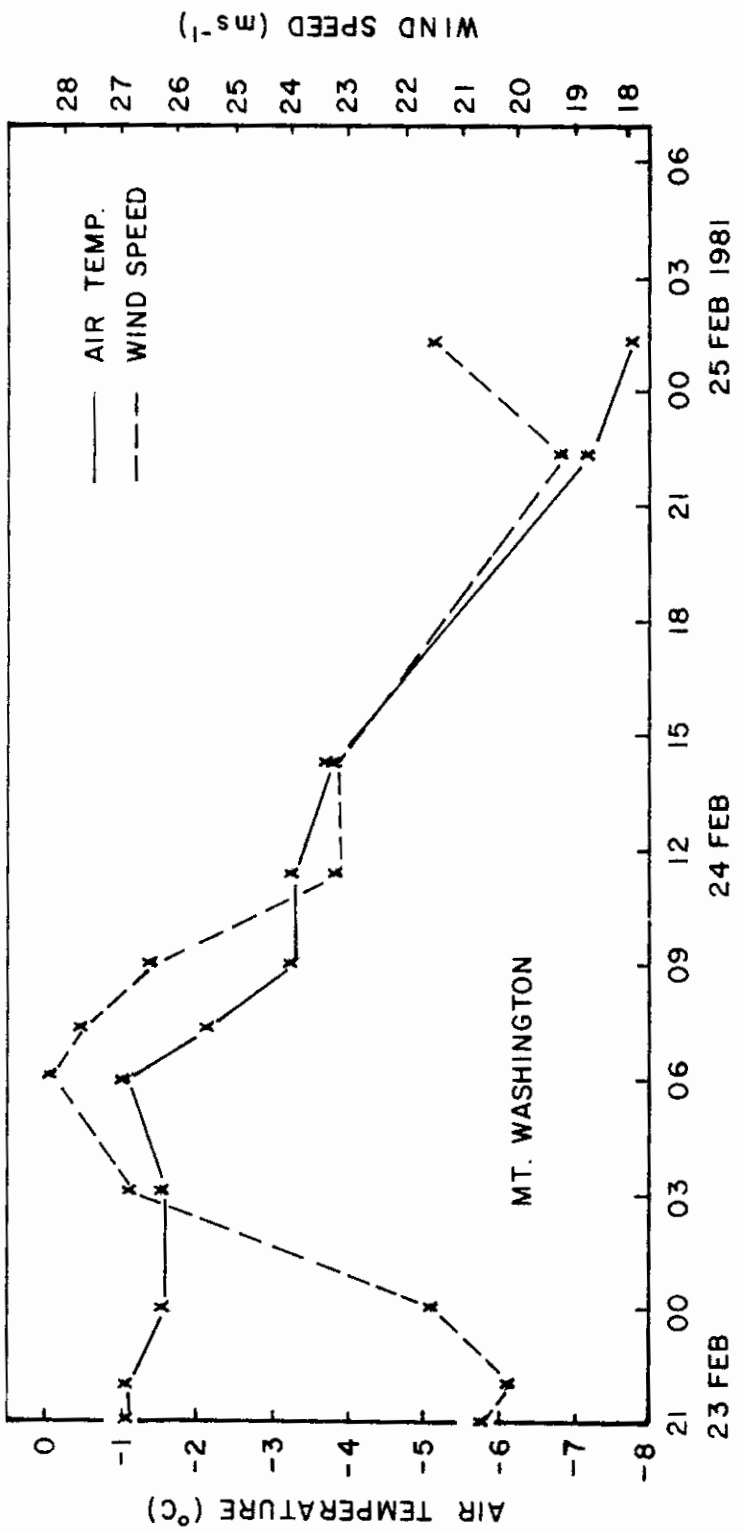

Fig. 20 Air temperature and wind speed on Mt. Washington 23-25 February 1981. Data from Reference 31.

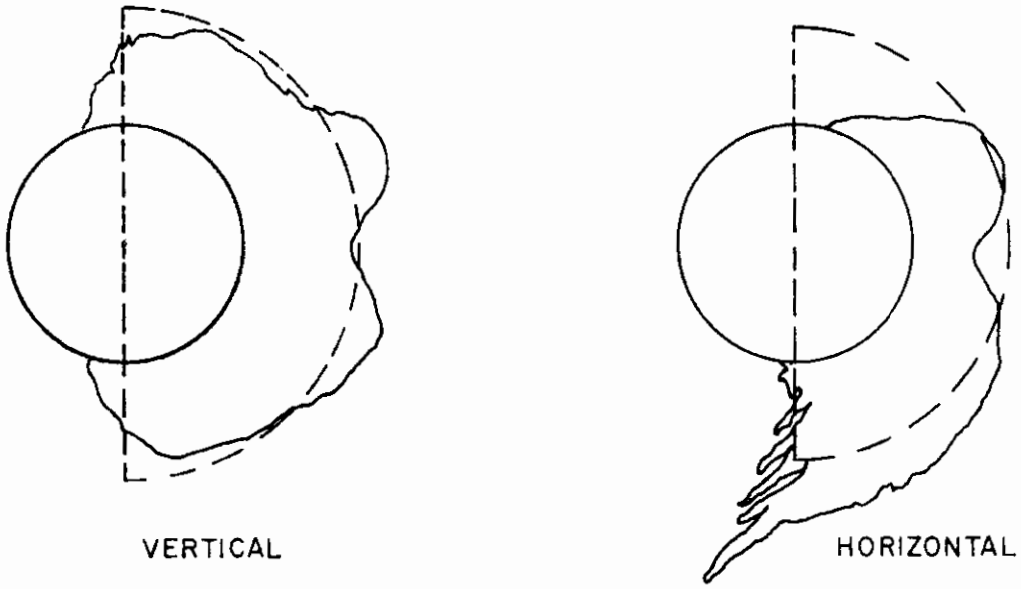

Fig. 21 Typical ice accretion shapes in the experiments of Reference 33 (solid lines), and the ice shape assumed on a fixed cylinder in the icing model (broken lines).

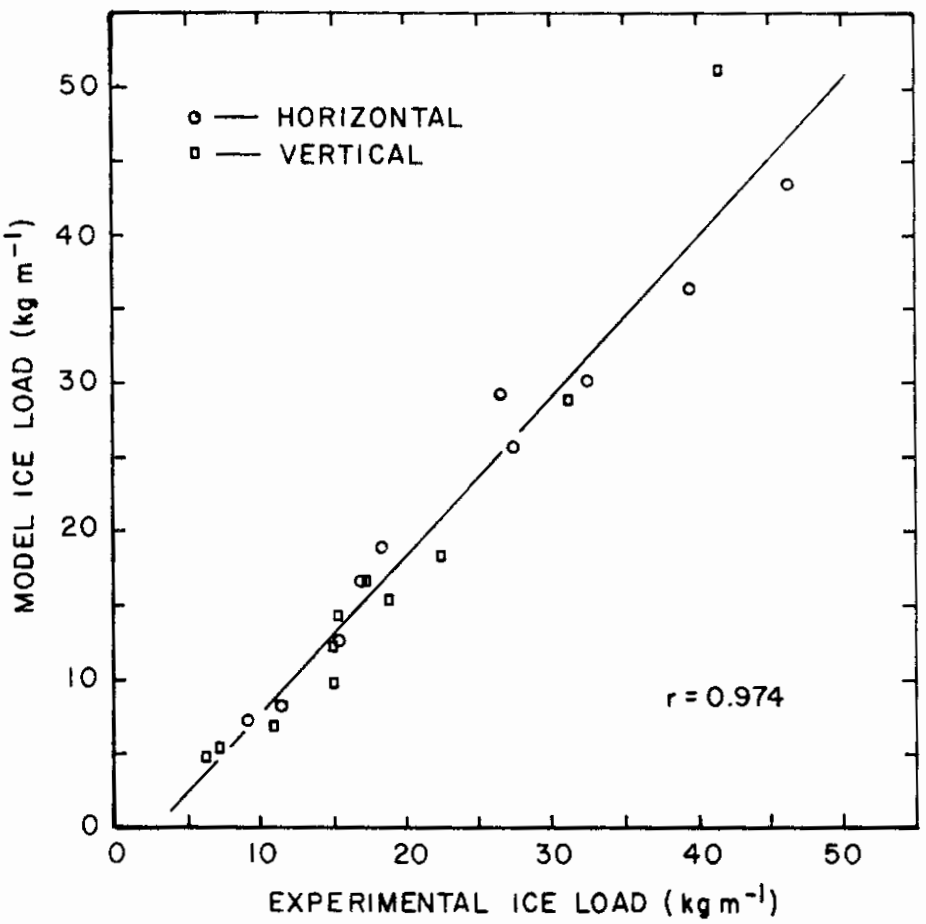

Fig. 22 Ice load on fixed cylinders predicted by the model vs. experimental ice load from Reference 33.

TABLE 1 Test Results and Model Predictions for the Rotating Cylinder Experiments

Test No.	Cylinder Diameter	Test Duration	Wind Velocity	Air Temp.	Liquid Water Content	Median Volume Droplet Diameter	EXPERIMENTS			MODEL PREDICTION		Theoretical Mean Collection Efficiency
							Ice Weight	Ice Density	Mean Collection Efficiency	Ice Weight	Ice Density	
	cm	min	ms^{-1}	°C	gm^{-3}	μm	g	$g\ cm^{-3}$		g	$g\ cm^{-3}$	
4	1.024	30	20	-4.5	0.36	17.1	9.34	0.87	0.56	9.45	0.84	0.57
5	1.024	30	20	-4.5	0.35	14.4	7.56	0.84	0.48	7.80	0.85	0.50
5E	1.024	30	20	-9.5	0.35	14.4	6.31	0.82	0.41	7.98	0.69	0.51
5F	1.024	30	20	-19.3	0.35	14.4	7.85	0.67	0.46	8.57	0.38	0.50
6	1.024	31	20	-4.5	0.33	13.1	6.54	0.84	0.46	6.71	0.85	0.47
9	3.183	40	20	-4.5	0.36	17.1	18.70	0.83	0.32	19.21	0.87	0.33
8	3.183	40	20	-4.5	0.35	14.4	14.18	0.75	0.25	14.31	0.77	0.26
8E	3.183	40	20	-9.5	0.35	14.4	12.44	0.74	0.23	14.41	0.45	0.26
8F	3.183	40	20	-19.3	0.35	14.4	13.46	0.48	0.24	14.58	0.22	0.26
7	3.183	40	20	-4.5	0.33	13.1	10.55	0.71	0.20	11.49	0.70	0.22
21	4.440	50	20	-4.5	0.36	17.1	23.17	0.78	0.23	25.12	0.82	0.25
20	4.440	50	20	-4.5	0.35	14.4	17.83	0.67	0.19	17.68	0.68	0.19
20E	4.440	50	20	-9.5	0.35	14.4	16.77	0.61	0.18	17.66	0.32	0.19
20F	4.440	50	20	-19.5	0.35	14.4	19.03	0.42	0.20	17.60	0.16	0.18
19	4.440	50	20	-4.5	0.33	13.1	11.91	0.63	0.14	13.52	0.51	0.15
22	7.609	50	20	-4.5	0.36	17.1	29.6	0.70	0.18	23.09	0.63	0.14
22E	7.609	50	20	-9.5	0.36	17.1	31.8	0.68	0.19	23.09	0.29	0.14
23	7.609	50	20	-4.5	0.35	14.4	15.2	0.63	0.10	12.78	0.29	0.08
23E	7.609	50	20	-9.5	0.35	14.4	17.3	0.50	0.11	12.57	0.14	0.08
23F	7.609	50	20	-19.3	0.35	14.4	19.1	0.30	0.12	12.53	0.10	0.08
24	7.609	50	20	-4.5	0.33	13.1	10.9	0.46	0.07	7.48	0.17	0.05
2	1.024	30	36	-4.9	0.15	15.7	7.42	0.88	0.63	7.44	0.92	0.64
1	1.024	30	36	-4.9	0.15	13.4	6.38	0.89	0.56	6.64	0.91	0.59
3	1.024	30	36	-4.9	0.14	12.2	5.39	0.88	0.50	5.95	0.89	0.55
10	3.183	40	36	-4.9	0.15	15.7	19.07	0.85	0.45	16.81	0.90	0.40
11	3.183	40	36	-4.9	0.15	13.4	13.59	0.82	0.33	13.83	0.85	0.33
12	3.183	40	36	-4.9	0.14	12.2	11.11	0.81	0.28	11.74	0.82	0.29
16	4.440	50	36	-4.9	0.15	15.7	26.65	0.84	0.35	22.83	0.87	0.32
17	4.440	50	36	-4.9	0.15	13.4	17.75	0.79	0.25	18.13	0.81	0.25
18	4.440	50	36	-4.9	0.14	12.2	12.30	0.80	0.18	14.97	0.75	0.22
15	7.609	50	36	-4.9	0.15	15.7	27.4	0.74	0.22	23.47	0.79	0.19
14	7.609	50	36	-4.3	0.15	13.4	16.7	0.76	0.14	16.68	0.70	0.14
13	7.609	50	36	-4.9	0.14	12.2	12.5	0.65	0.11	12.42	0.48	0.11

TABLE 2 Test Results and Model Predictions for the Wire Icing Experiments

Test No.	Wire Diameter	Spring Constant	Test Duration	Wind Velocity	Air Temp.	Liquid Water Content	Median Volume Droplet Diameter	EXPERIMENTS				MODEL PREDICTION		
								Ice Weight	Mean Radial Ice Thickness	Ice Density	Maximum Angle of Rotation	Ice Weight	Mean Radial Ice Thickness	Ice Density
	cm	Nm/rad	h	m/s	°C	g/m^3	μm	kg/m	cm	g/cm^3	°	kg/m	cm	g/cm^3
W1	0.95	7.6×10^{-3}	10	30	-4.7	0.32	13.6	3.56	4.0	0.57	1750	3.38	3.3	0.75
W2	0.95	7.6×10^{-3}	4	30	-9.7	0.32	13.6	1.18	2.1	0.58	890	1.32	2.0	0.72
W3	0.95	7.6×10^{-3}	4	20	-4.5	0.35	14.4	0.61	1.4	0.63	590	0.78	1.4	0.78
W4	0.95	7.6×10^{-3}	4	20	-4.5	0.23	12.3	0.47	1.2	0.57	485	0.41	0.9	0.75
W5	0.95	7.7×10^{-3}	4	20	-9.5	0.23	12.3	0.48	1.5	0.40	560	0.41	1.0	0.65
W6	4.02	9.6×10^{-3}	4	30	-4.3	0.32	13.6	1.40	1.5	0.54	455	1.43	1.2	0.76
W7	4.02	9.6×10^{-3}	4	30	-9.3	0.32	13.6	1.58	1.5	0.58	470	1.43	1.3	0.66
W8	4.02	9.6×10^{-3}	4	20	-4.3	0.23	12.3	0.53	0.8	0.45	260	0.40	0.4	0.63